

Heterogeneous Two-Region Model for Low-Aspect-Ratio Fixed-Bed Catalytic Reactors. Analysis of Fluid-Convective Contributions

Daniela A. Asensio,^{†,‡} Mariana T. Zambon,^{†,‡} Germán D. Mazza,^{*,†,‡} and Guillermo F. Barreto^{§,||}

[†]Instituto Multidisciplinario de Investigación y Desarrollo de la Patagonia Norte, IDEPA (CONICET—Universidad Nacional del Comahue), Buenos Aires 1400, Neuquén (8300), Argentina

[‡]Departamento de Ingeniería Química, Facultad de Ingeniería, Universidad Nacional del Comahue, Buenos Aires 1400, Neuquén (8300), Argentina

[§]PROIRQ, Departamento de Ingeniería Química, Facultad de Ingeniería, Universidad Nacional de La Plata (UNLP), Calle 47 No. 257, (1900) La Plata, Argentina

^{||}Centro de Investigación y Desarrollo en Ciencias Aplicadas “Dr. J.J. Ronco”, CINDECA (CONICET—Universidad Nacional de La Plata), (1900) La Plata, Argentina

ABSTRACT: A two-region, two-dimensional (2R2D) model aimed at improving the heat transfer description of multitubular catalytic reactors is introduced here. The effects concentrated in the wall thermal resistance ($1/h_w$) of the standard 2D model (S2D model) are distributed in a fluid channel from the wall up to a distance of half-particle diameter and in the particle layer against the wall. The use of computational fluid dynamics (CFD) on regular arrays allowed estimations of two of the 2R2D key parameters: the heat transfer coefficient between wall and core channels h_f and the “true” wall-to-fluid coefficient h_{wf} . The 2R2D and S2D models are compared at conditions when fluid mechanisms dominate radial heat exchange and reversible or irreversible catalytic reactions are carried out. The case of NH_3 synthesis was taken as a basis of comparison. Significant differences are obtained in temperature predictions within the usual range of the tube-to-particle diameter ratio, $5 < N < 10$, mainly for irreversible kinetics.

1. INTRODUCTION

Packed beds are extensively used in the field of process industry, in particular as fixed-bed reactors with conventional granular catalysts. When the process requires simultaneous heat exchange, multitubular packed-bed reactors presenting low aspect ratios ($N = D_t/D_p$) are used, being $5 \leq N \leq 10$ a typical range in industrial units.

Modeling and simulation of multitubular catalytic packed-bed reactors have been the objective of many studies in past decades. Temperature differences over the bed cross section in the range of tenths of degrees are usually developed. Due to the highly nonlinear dependence of catalytic reactions with temperature and frequently to safety reasons, it has been long ago acknowledged that two-dimensional (2D) models describing changes in radial and axial directions are necessary as a basis for mathematical simulation.

The standard 2D model (S2D model) describes radial heat transfer by means of an effective radial conductivity, λ_e , which along with axial velocity and bed voidage is assumed to be uniform over the cross section. As a steep drop/rise in temperature is observed close to the wall of the tube, the S2D model introduces a contact thermal resistance at the wall, normally expressed by its inverse: the wall heat transfer coefficient h_w . Pioneer research to evaluate h_w was made by Coverly and Marshall¹ and Brötz.² Since then, many other efforts have been made to measure and correlate both parameters, λ_e and h_w (it is noted that these thermal parameters enclose particle and fluid contributions or, equivalently, stagnant and convective contributions). Some relevant references on the estimation of λ_e and h_w have been discussed recently by Dixon.³ Although the

need for introducing h_w can be in principle justified by the existence of an unmixed film of fluid in contact with the wall, it has been recognized that additional effects arise as a consequence of the arrangement of particles close to the wall. Thus, a highly ordered layer of particles, especially for monosized spherical particles, can be identified against the wall surface. The ordering effect of the wall is attenuated toward the interior of the bed until a virtual random packing is reached, as can be appreciated in Figure 1 in terms of a void-fraction profile $\varepsilon(y^*)$, with y^* being the distance from the wall measured in units of D_p , from experimental data of Mueller⁴ and also from a bed packing simulation from Salvat et al.⁵ Concomitant profiles of the axial superficial velocities $u(y^*)$ arise, such as those depicted in Figure 2 from the experimental data of Giese et al.⁶ Roughly, $u(y^*)$ follows the attenuated wave defining $\varepsilon(y^*)$, except for the existence of a sharp maximum very close to the wall.

The organized packing near the wall and the induced variations of the velocity field impair radial heat transfer mechanisms and thermal resistances along a finite distance from the wall arise, in addition to that of an unmixed fluid film just against the tube wall. In the S2D, all these effects are accounted for by h_w , and therefore its evaluation becomes strongly dependent on the specific measurement techniques and experimental conditions, facts that are responsible for the general dispersion of results. Only at high Re_p numbers the effect of the

Received: September 29, 2013

Revised: December 30, 2013

Accepted: February 6, 2014

Published: February 21, 2014

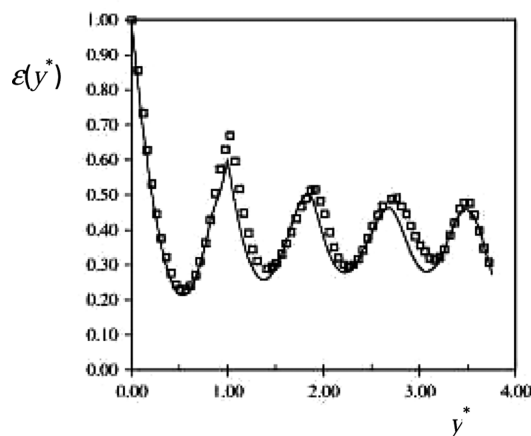


Figure 1. Experimental (symbols, Mueller⁴) and predicted (continuous curve, Salvat et al.⁵) void fraction radial profiles at $N = 7.99$.

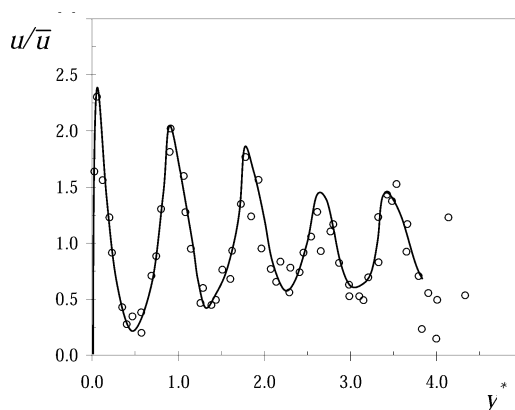


Figure 2. Local superficial axial velocity measured by Giese et al.⁶ at $Re_p = 532$ and $N = 9.3$. The continuous line is a trend curve.

unmixed film dominates and Nu_w (the corresponding Nusselt number of h_w) can be correlated reasonably well with the Re_p number (see, e.g., ref 7), but the data are strongly dispersed for moderate or low Re_p (less than around 500; see, e.g., ref 8), when the different effects operate simultaneously on Nu_w .

Such dispersion of data for Nu_w has raised controversy about the usefulness of the S2D model. According to some authors, noticeably Tsotsas and Schlünder,⁷ the S2D model and the use of h_w should be abandoned in favor of models with variable effective thermal conductivity. On the other hand, efforts leading to obtain careful experimental results and proper accounting of the mechanisms that h_w represents are believed to make possible the development of useful correlations for Nu_w , as recently discussed by Dixon.³

Provided that proper values of h_w and λ_e can be assessed, the S2D model will correctly predict the heat flux to the wall when the fixed bed is operated strictly as a heat exchanger (without heat reaction effects), even when the temperature profile close to the wall cannot be evaluated with precision. However, when a catalytic reactor is to be simulated, the temperature profile gains in significance, as heat exchange is basically intended for removing/providing the strongly temperature-dependent heat involved in the catalytic reactions, rather than cooling/heating the fluid stream.

Following the purpose of achieving a conceptually better description of the heat transfer mechanisms or motivated by the S2D limitations in simulating catalytic packed bed reactors,

several models intending to disaggregate the effects lumped in the parameter h_w of the S2D model have been put forward in the literature. These models will be referred to here as *two-region two-dimensional* (2R2D) models, and some representative examples will be briefly described in section 2.

The main objective of this paper is to present a new heterogeneous 2R2D model for packed beds of spherical catalytic particles with gas flow. The model is intended for correcting the most significant deficiencies of the S2D model by identification of the largest thermal resistances caused by the wall itself and the ordered layer of particles against the wall (first particle layer). Hence, two channels for fluid flow are identified, with the boundary at $D_p/2$, where heat (and mass) is strongly restrained, and the first particle layer is explicitly recognized. Similarities and differences between the proposed and precedent models are discussed in section 2.

2. SURVEY OF 2R2D MODELS

The 2R2D models intend to disaggregate the effects lumped in the parameter h_w of the S2D model. To this end, the effects are distributed over a finite portion of the bed cross section, which will be called *wall region*. The rest of the bed, up to the bed axis, is defined as the *core region*, whose thermal behavior is modeled with uniform properties, much in the same way as in the S2D model. In this sense, one exception is set by the formulation of Ahmed and Fahien,¹⁰ which uses variable effective thermal conductivity in the core region, $\lambda_{e,c}$.

A representative list of 2R2D models is given in Table 1, together with some relevant features shown by each of them.

Table 1. Main Features of Several 2R2D Models Proposed in the Literature

reference	radial heat transfer parameters in wall region	extent of wall region
Botterill and Denloye ¹¹	$1/h_w$ (concentrated), uniform λ_e	$y_w^* = 1/2$ (jump to reach $\lambda_{e,c}$)
Ahmed and Fahien ¹⁰	linear profile $\lambda_e(y^*)$ between $\sim \lambda_f$ and $\lambda_{e,c}$	$y_w^* = 2$ [$\lambda_e(y^*)$ reaches $\lambda_{e,c}$]
Gunn et al. ¹²	$1/h_w$ (covering a finite distance y_w^* from the wall)	$y_w^* = 0.3$
Borkink and Westertep ¹³	$1/h_w$ (concentrated), uniform λ_e	$3/4 < y_w^*(N) < 5/4$ (jump to reach $\lambda_{e,c}$)
Legawiec and Ziółkowski ¹⁴	<i>fluid</i> : $1/h_{wf}$ (concentrated), λ_{ef} piecewise constant in four subregions <i>solid</i> : conduction in three particle layers of thickness D_p and gas-fillet resistances in between	$y_w^* = 3.5$ (jump to reach $\lambda_{ef,c}$) $y_w^* = 3.0$ (to start using $\lambda_{es,c}$)
Winterberg et al. ¹⁵	$\lambda_e(y^*) = \lambda_{eD}(e(y^*)) + \lambda_{eD}(y^*)$, quadratic profile $\lambda_{eD}(y^*)$, between 0 and $\lambda_{eD,c}$	$y_w^* = 2$ ($Re_p = 66$) $y_w^* \approx 0.44$ ($Re_p > 500$) [$\lambda_{eD}(y^*)$ reaches $\lambda_{eD,c}$] $y_w^* \approx 1$ [$\lambda_{eD}(y^*)$ reaches $\lambda_{eD,c}$]
Smirnov et al. ¹⁶	$1/h_w$ (covering a finite distance y_w^* from the wall)	$y_w^* = 0.25$

Only the model of Legawiec and Ziółkowski¹⁴ makes a distinction between fluid and particle temperatures; i.e., it is a heterogeneous model. In spite of further complexity, this is believed to be a desirable feature, since significant temperature differences in the wall region can be expected (even without catalytic reactions), as a consequence of the heat source/sink represented by the wall and also because of different heat transfer capacities of both phases. For example, computational fluid

dynamics (CFD) calculations by Magnico¹⁷ clearly show those differences. In the remaining 2R2D models the effective conductivity is evaluated as $\lambda_e = \lambda_{e0} + \lambda_{eD}$, where λ_{e0} is the static contribution (without fluid flow) and λ_{eD} is the dispersion contribution due to lateral fluid mixing.^{18,19}

Most 2R2D models are basically formulated for monosized (near) spherical particles. Instead, Winterberg and Tsotsas²⁰ provide a specific formulation for cylinders and Gunn et al.¹² and Smirnov et al.¹⁶ approaches were used by the authors to simulate experiments with cylinders.

The 2R2D models widely differ in the description of properties in the wall region, as can be appreciated in Table 1 for the thermal parameters. On one hand, some models^{10,15} eliminate the use of h_w by employing in the wall region a decreasing variation of λ_e up to a value close to λ_f at $y^* = 0$. In the remaining models h_w is kept under the conception that it represents a thin film of unmixed fluid in contact with the wall. As can be appreciated in Table 1, the modification to the S2D model proposed by Gunn et al.¹² and Smirnov et al.¹⁶ just consists in assigning a finite region to the thermal resistance $1/h_w$.

A common definition of the wall region y_w^* cannot be made for all models in Table 1. For the just mentioned two models, y_w^* can be assigned to the extent covered by $1/h_w$, which is defined by fitting experimental data. For the remaining models, y_w^* can be assigned to the thickness of the regions in which the effective thermal conductivity is allowed to change. In this way, a wide range for y_w^* arises: $0.25 < y_w^* < 3.5$ (Table 1).

On the other hand, the 2R2D models listed in Table 1 use different values of void fraction and superficial velocity in the wall region (continuously varying or piecewise constant), with exceptions of the Gunn et al.¹² and Smirnov et al.¹⁶ approaches.

In spite of their differences, all the 2R2D models are shown to describe better temperature profiles than the S2D model—as shown in the original publications—for heat transfer experiments without chemical reactions. Therefore, it seems that prediction of temperature profiles close to the wall can be improved if a reasonable spatial distribution of the thermal resistance is provided. Only the models of Ahmed and Fahien¹⁰ and Winterberg et al.¹⁵ were tried by the authors for simulating a limited number of experimental tests under catalytic reaction conditions.

The 2R2D model introduced in this paper distinguishes between fluid and solid temperatures and is intended for packed beds of spherical catalytic particles.

Considering that conduction through the solid particles is relatively fast, the main resistances for heat transfer in the first particle layer are imposed by the thin films of fluid surrounding the contact point of each particle with the wall and the contact points with inner particles. Then, only two temperature levels are considered within the particle layer.

Radial dispersion of fluid contributing to heat transport is suppressed at the wall and strongly restrained around $y^* = 1/2$, where the fluid is essentially confined by surrounding particles and consequently shows little motion, as revealed by very low superficial axial velocities (Figure 2). Then, a wall channel for fluid flow is identified from the wall up to a distance $y^* = 1/2$, where the mixing-cup average temperature will represent the thermal level of the fluid, and two concentrated thermal resistances are considered: one at the wall (unmixed fluid film on the wall) quantified by $1/h_{wf}$ and the other at $y^* = 1/2$ quantified by $1/h_f$, where h_f is the heat exchange coefficient between the fluid in the wall channel and in the core region.

The remains of the bed, comprising the fluid at $y^* > 1/2$ and particles other than those in the first layer, constitutes the core region, which is basically treated as in the S2D model. Nonetheless, a heterogeneous description discriminating fluid and solid temperatures is maintained for consistency with the wall region and both, solid and fluid phase, are assumed as pseudocontinuous media. Different values of superficial velocity and void fraction are assumed in the regions $0 < y^* < 1/2$ and $y^* > 1/2$. The model is further conceptualized and formulated in section 3.

The main differences from most previous 2R2D models are the following:

1. An heterogeneous thermal description for solid and fluid phases is considered (this feature is shared with Legawiec and Ziółkowski's model, Table 1).

2. It is recognized that radial fluid-dispersion contribution to heat transfer presents two minimum (at $y^* = 0$ and $y^* = 1/2$) within a distance of $1D_p$ from the wall. In the 2R2D models that discriminate this contribution, a decreasing trend toward the wall was always considered in the wall region.

3. No adjustable spatial parameter is introduced to define the wall region, as the heat transfer mechanisms are directly related to the bed structure near the wall. This feature is expected to facilitate the development of reliable correlations for heat transfer parameters.

The concept of a significant thermal resistance at $D_p/2$ between the wall channel and the fluid in the core region has been employed in some previous papers. Mariani et al.²¹ used both parameters, h_{wf} and h_f , for the liquid phase in trickle beds, and in this way they could successfully interpret heat transfer rates measured at low aspect ratios N . Martin²² employed the concept to analyze fluid to particle heat transfer data, although Martin assumed the heat exchange coefficient h_f as being directly nil. Yagi and Kunii²³ expressed the (overall) wall heat transfer coefficient in terms of several thermal resistances, and one of them can be assimilated to $1/h_f$.

3. FORMULATION OF THE PROPOSED 2R2D MODEL

The sketch in Figure 3 will be employed to describe the proposed 2R2D model, for which spherical particles of uniform diameter D_p in a cylindrical container of diameter D_t are assumed.

Some aspects of the formulation will be restrained to values $N \geq 5$.

3.1. Distribution of Particles and Fluid Flow in the Bed Cross Section.

In order to visualize the accommodation of particles close to the wall, the distribution of particle centers from random packing simulation⁵ in a $N = 5.04$ bed is presented in Figure 4. The outer neatly defined ring of particle centers is at $y^* = 1/2$, and essentially all particles are touching the wall. They are defined as those pertaining to the first particle layer. A significant dispersion is observed for the centers in the second layer and some particle centers around $y^* = 1$ can be observed between both layers, while virtually no center is observed in the middle zone, say $1/2 < y^* < 0.9$. These results are completely in line with the observations of Legawiec and Ziółkowski,²⁴ who further evaluated that centers at around $y^* = 1$ amount to $\sim 10\%$ of those in the first layer. Those particles are the main cause of some defects in the arrangement of the first particle layer, as can be visualized in Figure 5.

In the following, according to convenience, the radial position will be described by either the dimensionless distance y^* from the wall or by the radial coordinate ρ , noting that $\rho = \rho_t - D_p y^*$, where $\rho_t = D_t/2$.

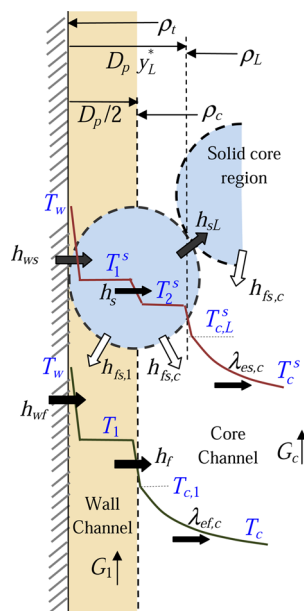


Figure 3. Sketch for the 2R2D model introduced in this paper. The contour of the particle touching the wall represents the first particle layer. The schematic fluid and particle temperature profiles are drawn at different levels.

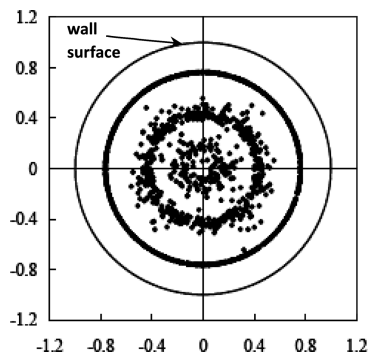


Figure 4. Distribution of particle centers from bed packing simulation using Salvat et al.⁵ algorithm for $N = 5.04$. Cartesian coordinates normalized with tube radius.

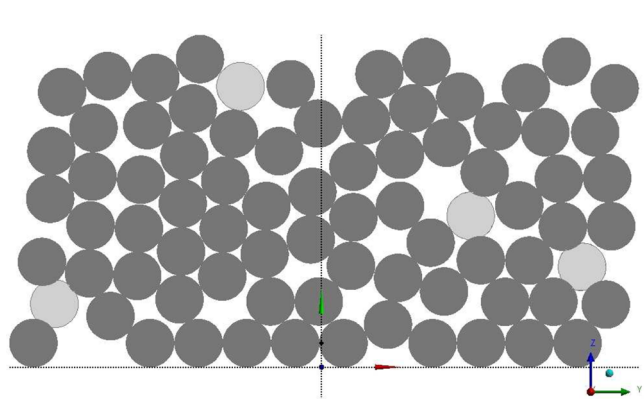


Figure 5. Projections of spheres with centers at $1/2 \leq y^* \leq 1$ onto the plane, from bed packing simulation using Salvat et al.⁵ algorithm for $N = 5.04$ and a bed height of nearly $6D_p$. Dark circles correspond to spheres touching the wall, and light circles correspond to spheres with centers close to $y^* = 1$.

The number of particle centers in the first layer ($y^* = 1/2$) per unit area of the cylindrical surface of radius $\rho_c = \rho_t - D_p/2$ (see Figure 3) is defined as n_p . According to the analysis of Mariani et al.,²⁵ the normalized density $n_p^* = n_p D_p^2$ is relatively insensitive to values of the aspect ratio N when $N \geq 5$ and is very close to unity.

Figure 5 is also useful for visualizing the confinement of the fluid around $y^* = 1/2$ in the openings left by the particles of the first layer, as discussed in section 1, with very restrained fluid motion (see Figure 2). The wall channel can be defined by the region between the wall and the position y_{min}^* of the minimum local voidage. For particles touching the wall, y_{min}^* is slightly larger than $1/2$ at small N , because of curvature effects. For the same reason, the fraction ω of particle volume intersected between the wall and y_{min}^* is somewhat larger than $V_p/2$. Restrained to values $N > 5$, we will approximate $y_{min}^* = 1/2$ and the fraction ω at this position can be approximately evaluated as

$$\omega = 0.5(1 + 0.3/N) \tag{1}$$

The average voidage ϵ_1 of the channel region $0 < y^* < 1/2$ ($\rho_c < \rho$) can now be evaluated from

$$(1 - \epsilon_1)(\rho_t^2 - \rho_c^2) = \omega n_p \left(\frac{\pi}{6} D_p^3 \right) 2\rho_c \tag{2a}$$

In dimensionless terms,

$$(1 - \epsilon_1) \left(N - \frac{1}{2} \right) = \omega \frac{\pi}{3} n_p^* (N - 1) \tag{2b}$$

The average axial superficial mass velocity of the fluid in the wall channel will be denoted by G_1 . Hence, the fluid flow in the wall channel is $G_1 \pi (\rho_t^2 - \rho_c^2) = G_1 (\pi/4) D_p^2 (2N - 1)$. As regards the fluid flow, the remaining part of the bed ($y^* > 1/2$) is defined as the *core channel*, where the axial average superficial mass velocity is G_c and the average voidage is ϵ_c . The ratio G_1/G_c is a model parameter, which in principle can be estimated from literature information (e.g., refs 6 and 26). On the other hand, ϵ_c can be calculated by subtracting the solid volume in the wall channel from the total solid volume in the bed:

$$(1 - \epsilon_c) \rho_c^2 = (1 - \epsilon) \rho_t^2 - \omega n_p \left(\frac{\pi}{6} D_p^3 \right) 2\rho_c \tag{3a}$$

where ϵ is the average bed voidage. Using eq 2a to replace n_p and expressing in dimensionless terms

$$(1 - \epsilon_c)(N - 1)^2 = (1 - \epsilon)N^2 - (1 - \epsilon_1)(2N - 1) \tag{3b}$$

Given N and values of a pair of properties related to particle distribution (e.g., ϵ and n_p^*), the remaining two properties (e.g., ϵ_c and ϵ_1) will be determined with the use of eqs 2b and 3b.

Now, as stated in the Introduction, particles other than those in the first layer will be treated as a pseudocontinuous phase with uniform properties (*solid core region*). To determine the distance y_L^* at which the solid core region begins (see Figure 3), the volume of particles within $0 < \rho < \rho_L = \rho_t - D_p y_L^*$ is equated to the difference between the total volume of particles and the volume of the first particle layer. Assuming that the voidage in $0 < \rho < \rho_L$ is ϵ_c , we can write

$$(1 - \epsilon_c) \rho_L^2 = (1 - \epsilon) \rho_t^2 - n_p \left(\frac{\pi}{6} D_p^3 \right) 2\rho_c \tag{4a}$$

Alternatively, using eq 2a to replace n_p and expressing in dimensionless terms

$$(1 - \varepsilon_c)(N - 2y_L^*)^2 = (1 - \varepsilon)N^2 - (1 - \varepsilon_c)(2N - 1)/\omega \quad (4b)$$

Usual values of y_L^* from eq 4b are in the range 0.85–0.95.

A useful geometrical interpretation of y_L^* arises by considering a bed of large $N \rightarrow \infty$ built up from particle layers identical to the first one, which keep uniform spacing L . Then, eliminating the term in $1 - \varepsilon$ between eqs 3a and 4a and taking $N = D_t/D_p \rightarrow \infty$ and $\omega \rightarrow 1/2$ in the result, $(1 - \varepsilon_c)L/D_p = (\pi/6)n_p^*$ is finally obtained, with $L/D_p = (2y_L^* - 1)$. Furthermore, assuming that the separation between layers is determined by the contact between particles of neighboring layers, L is also the distance between consecutive planes containing contact points. Thus, it is concluded that for the described case y_L^* corresponds to the distance from the wall at which particles of the first layer maintain contact with inner particles. Although approximate for cylindrical beds of finite N , this interpretation for y_L^* is significant, as the particle temperature suffers a jump around contact points and therefore it seems to be the natural boundary between the first particle layer and the solid core region.

We can appreciate in Figure 3 that at both sides of y_L^* small spherical caps of particles in the first layer get into the solid core region and vice versa. The assumption of a boundary between the two particle regions implicitly moves the volume of the caps inside their own zones. Although in this way heat exchange between the solids and fluid will be modified, the effect should be of no practical consequence, due to the small volume of the caps and their short spatial reallocation.

It is convenient to stress that in both intervals, $0 < \rho < \rho_L$ (solid core region) and $0 < \rho < \rho_c$ (core channel), the void fractions have been assumed to be ε_c . Therefore, in the intermediate zone $\rho_L < \rho < \rho_c$ the void fraction will be also ε_c .

3.2. Heat and Mass Conservation Equations. A lumped description is adopted for the thermal behavior in the wall channel (mixing-cup average temperature T_1 , see Figure 3). The fraction of the external surface of particles in the first layer exchanging heat with the fluid in wall channel is assumed to be ω , i.e., the same as the particle volume fraction in the wall channel, and the surface average temperature on fraction ω is T_1^s . The remaining fraction $1 - \omega$ exchanges heat with the fluid in the core channel within $1/2 < y^* < y_L^*$, and the surface average temperature on the fraction $1 - \omega$ is T_2^s (Figure 3).

Distributed temperature profiles are used for the core channel, $T_c(\rho)$, and solid core region, $T_c^s(\rho)$ (particle surface temperature); see Figure 3.

The proposed heat exchange mechanisms between the solid and fluid regions and their parameters are summarized in the sketch of Figure 3.

The surface areas on which the heat transfer/exchange coefficients are defined are as follows:

$$\begin{aligned} h_{wf}, h_{ws}: & \text{ wall surface, } \rho = \rho_t \text{ (} y^* = 0 \text{)} \\ h_f, h_s: & \text{ cylindrical surface at } \rho = \rho_c \text{ (} y^* = 1/2 \text{)} \\ h_{sL}: & \text{ cylindrical surface at } \rho = \rho_L \text{ (} y^* = y_L^* \text{)} \\ h_{fs,1}, h_{fs,c}: & \text{ external particle surface} \end{aligned}$$

Both coefficients h_{ws} and h_{sL} are assumed to include the thermal resistance inside the particles.

Mass conservation equations in the fluid flowing in both wall and core channels for a species (molar concentration C) undergoing a catalytic reaction with effective rate r_e and heat of reaction ΔH will also be formulated. It is assumed that $r_e(T^s, C^s)$ stands for the effective reaction rate evaluated by assuming a spherical particle of D_p with uniform temperature and

concentration (T^s and C^s) on its external surface. The formulation for evaluating $r_e(T^s, C^s)$ is not written here as it is standard, but it is noted that any temperature departure inside the particle from T^s can also be accounted for in evaluating r_e .

Following similar arguments that were employed for heat exchange, a concentrated mass transfer resistance ($1/\alpha_f$) at $y^* = 1/2$ is assumed to cause significant differences between concentrations in both channels (C_1 and $C_{c,1}$). In turn, different particle-surface values arise: C_1^s on the fraction ω and C_2^s on the fraction $1 - \omega$. The analogy between heat and mass transfer can be employed to evaluate α_f from a known value of h_f (see section 4). Fluid/particle mass transfer coefficients $\alpha_{fs,1}$ and $\alpha_{fs,c}$ are also related to the analogous heat transfer coefficients $h_{fs,1}$ and $h_{fs,c}$ (see Figure 3).

Following the previous considerations and on the basis of the sketch in Figure 3, the thermal and mass conservation balances written for steady state conditions and ignoring axial dispersion/conduction effects can be expressed in the following ways:

In the *wall channel*:

$$c_{pf}G_1 \frac{dT_1}{dz} = (1 - \varepsilon_1) \frac{6h_{fs,1}(T_1^s - T_1)}{D_p} + \frac{2\rho_t h_{wf}(T_w - T_1) + 2\rho_c h_f(T_{c,1} - T_1)}{\rho_t^2 - \rho_c^2} \quad (5a)$$

$$G_1 \frac{d(C_1/\delta_f)}{dz} = (1 - \varepsilon_1) \frac{6\alpha_{fs,1}(C_1^s - C_1)}{D_p} + \frac{2\rho_c \alpha_f(C_{c,1} - C_1)}{\rho_t^2 - \rho_c^2} \quad (5b)$$

In the *first particle layer*, sides ω and $1 - \omega$:

$$(1 - \varepsilon_1)(\rho_t^2 - \rho_c^2) \left[(-\Delta H)r_e(T_1^s, C_1^s) - \frac{6h_{fs,1}(T_1^s - T_1)}{D_p} \right] = 2\rho_t h_{ws}(T_1^s - T_w) + 2\rho_c h_s(T_1^s - T_2^s) \quad (6a)$$

$$(1 - \varepsilon_c)(\rho_c^2 - \rho_L^2) \left[(-\Delta H)r_e(T_2^s, C_2^s) - \frac{6h_{fs,c}(T_2^s - T_2)}{D_p} \right] = 2\rho_L h_{sL}(T_2^s - T_{c,L}^s) + 2\rho_c h_s(T_2^s - T_1^s) \quad (6b)$$

In eq 6b T_2 is the average value of T_c in the cross section zone defined by $1/2 < y^* < y_L^*$ (Figure 3), i.e., $\rho_L < \rho < \rho_c$.

In the *core channel* ($y^* > 1/2, \rho < \rho_c$):

$$-\lambda_{ef,c} \frac{\partial(\rho \partial T_c / \partial \rho)}{\rho \partial \rho} + c_{pf}G_c \frac{\partial T_c}{\partial z} = (1 - \varepsilon_c) \frac{6h_{fs,c}(T^s - T_c)}{D_p} \quad (7a)$$

$$-D_{e,c} \frac{\partial(\rho \partial C_c / \partial \rho)}{\rho \partial \rho} + G_c \frac{\partial(C_c/\delta_f)}{\partial z} = (1 - \varepsilon_c) \frac{6\alpha_{fs,c}(C^s - C_c)}{D_p} \quad (7b)$$

at $\rho = \rho_c$:

$$\begin{aligned} T_c &= T_{c,1}, & -\lambda_{ef,c} \frac{\partial T_c}{\partial \rho} &= h_f(T_{c,1} - T_1) \\ C_c &= C_{c,1}, & -D_{e,c} \frac{\partial C_c}{\partial \rho} &= \alpha_f(C_{c,1} - C_1) \end{aligned} \quad (7c)$$

In eqs 7a and 7b

$$(T^s, C^s) = \begin{cases} (T_c^s, C_c^s) & \text{if } \rho < \rho_L \\ (T_2^s, C_2^s) & \text{if } \rho_L < \rho < \rho_c \end{cases} \quad (7d)$$

In the solid core region ($y^* > y_L^*$, $\rho < \rho_L$):

$$\begin{aligned} &-\lambda_{es,c} \frac{\partial(\rho \partial T_c^s / \partial \rho)}{\rho \partial \rho} \\ &= (1 - \varepsilon_c) \left[\frac{6h_{fs,c}}{D_p} (T_c - T_c^s) + (-\Delta H)r_e(T_c^s, C_c^s) \right] \end{aligned} \quad (8a)$$

$$T_c^s = T_{c,L}^s, \quad -\lambda_{es,c} \frac{\partial T_c^s}{\partial \rho} = h_{sL}(T_{c,L}^s - T_2^s), \quad \text{at } \rho = \rho_L \quad (8b)$$

For evaluating the particle-surface concentration C^s

$$r_e(T^s, C^s) = \frac{6\alpha_{fs}}{D_p} (C - C^s) \quad (9)$$

where $C = C_1$ in the wall channel or $C = C_c$ in the core channel. The heat flux at the wall is evaluated from

$$q_w = h_{wf}(T_1 - T_w) + h_{ws}(T_1^s - T_w) \quad (10)$$

It is clear from the spatial definition of the core regions that fluid and solid present different radial extents (from $y^* = 1/2$ and $y^* = y_L^*$, respectively), and so do their differential equations, eqs 7a, 7b, and 8a. This spatial mismatch may be uneasy for the numerical solution of the problem. An alternative for equating the domains of the differential equations is to use a lumped description for T_c and C_c in the range $1/2 < y^* < y_L^*$. The modified formulation, which does not add any new parameter, is given in Appendix A.

3.3. Discussion on Major Assumptions and Thermal Parameters Introduced in the Proposed Model. The proposed model is based on identifying the first particle layer and the effects that it causes on fluid flow distribution, on radial dispersion, and, consequently, on heat (and mass) transfer mechanisms. It is reasonable to think that a similar treatment could have been given to the second layer of particles. A first point to remark in this regard is the fact that the second layer is considerably more dispersed than the first one, as revealed by the distribution of particle centers (see Figure 3). According to Mariani et al.,²⁵ the centers can be assumed to be uniformly distributed between $1.2 < y^* < 1.5$. Therefore, the fluid can find some paths to flow in this zone. Actually, minimal axial superficial velocities nearly double the corresponding values at around $y^* = 1/2$ (see Figure 2). Radial dispersion will also take place more significantly than in the zone around $y^* = 1/2$, due to deflection of the streamlines, and it can be expected that radial dispersion of heat will be more effective than evaluated by the heat exchange coefficient h_f . Heat conduction through particles of the second layer will be also more effective than in the first particle layer, due

to the larger number of contact points between particles than the single contact point with the wall. If, in addition to the enhanced mechanisms, it is considered that temperature variations at the level of the second particle layer will be smaller than in the first layer zone, it can be concluded that a more detailed description of heat transfer in the second layer would most probably be of second order of importance.

In neglecting further details for the proposed model, we also took into account the practical difficulty in evaluating new parameters that should be additionally introduced. Also, as clearly noted by Borkink and Westerterp,¹³ upscaled models of the type considered here will be ultimately inappropriate at conditions when catalytic reactors show high parametric sensitivity, thus making unsound any effort for introducing a higher degree of complexity. CFD provides a possibility to deal successfully with such cases.

In the first particle layer two temperature levels were introduced, T_1^s and T_2^s . This discrimination was made because large temperature variations may take place across the particles at high heat transfer rates. As a consequence, a heat exchange coefficient h_s between the frontal fraction ω and back fraction $1 - \omega$ of the particles has to be introduced. A simple expression for h_s , derived in Appendix B (see eqs B5a–B5c) is thought to be accurate enough, provided that $T_1^s - T_2^s$ does not turn out to be very large.

The use of particle-surface average temperatures (T_1^s and T_2^s for particles in the first layer and T_c^s in the core region) instead of particle-volume average temperatures deserves some explanation. This choice allows evaluating fluid to particle heat exchange on the basis of coefficients $h_{fs,1}$ (in the wall channel) and $h_{fs,c}$ (in the core channel), strictly accounting for the thermal resistance on the fluid side. Otherwise, the use of particle-volume average temperatures will need associated heat transfer coefficients including the thermal resistance inside the particles. It is also noted at this point that the distinction made for h_{fs} in both fluid channels ($h_{fs,1}$ and $h_{fs,c}$) is made on account of different superficial velocities, voidage, and geometrical configurations. Expressions as that of Gunn²⁷ or that presented by Martin²² introducing the effect of void fraction may be useful in this regard.

The energy conservation equations in the solids (eqs 6a, 6b, 8a, and 8b) are written under the assumption that heat exchange between the wall and particle and between particles can be expressed with the same underlying heat transfer parameters (h_{ws} , h_{sL} , and $\lambda_{es,c}$) as in the case of heat transfer in a stagnant bed without chemical reactions. This is an approximation because these parameter values are associated with certain temperature distributions inside the particles, which will be modified as a consequence of simultaneous heat transfer with the fluid stream and reaction heat effects. At high Re_p , however, the fluid convective mechanism will dominate and such an approximation will be of lesser importance. On the contrary, conditions at low Re_p involve low heat exchange rate with the fluid and, in practice, low rates of chemical reaction heat generation. Then, wall/particle/particle heat exchange will dominate and heat transfer rates will be well estimated by using standard correlations for h_{ws} , h_{sL} , and $\lambda_{es,c}$. In any case, uncertainties will be lower for higher particle thermal conductivities, as milder temperature changes inside the particles will arise.

The expression analyzed by Bauer and Schlünder²⁸ is regarded as a reliable tool to estimate $\lambda_{es,c}$. Besides, h_{sL} can be written in terms of $\lambda_{es,c}$ as discussed in Appendix B (see eqs B7b and B8), where the evaluation of h_{ws} is also discussed (see eq B7a).

The remaining thermal parameters of the model are those accounting for radial heat transport through the fluid phase, h_{wf} , h_{β} and $\lambda_{ef,c}$. Except at very low Re_p when conduction is the dominant heat transfer mechanism, a coherent set of expressions for h_{wf} , h_{β} and $\lambda_{ef,c}$ describing the effect of fluid convection will be paramount for accurate predictions. Available correlations for h_{wf} are not straightforwardly appropriated for the proposed model. Most of them are developed on the basis of the S2D model, and the effect of the thermal resistance $1/h_f$ identified in the proposed model should mainly be included in values $1/h_{wf}$ from such correlations. If the dispersion of available data for h_w is recalled, as mentioned in the Introduction, it seems that any effort to extract values of h_f from literature information on h_w will be fruitless.

From section 3.1, where geometrical parameters of the model were introduced, and the discussion given above, it can be concluded that most parameters of the 2R2D model presented here have been studied in the literature and estimations to them from different sources are available. An exception to this picture is given by the couple h_{wf} and h_f . Preliminary efforts for estimating them in regular arrays of particles are presented in section 4, and their significance is discussed in the rest of this paper. Further studies on them in random packed beds are under way. The final stage in our planning is the assemblage of new and old parameters to obtain a reliable set for modeling packed-bed reactors.

Preliminary estimations of h_f and concomitant values of h_{wf} obtained from CFD calculations will be reported in section 4.

4. CFD EVALUATIONS

Evaluation of coefficients h_{wf} and h_f representing heat exchange in the wall channel and the ratio G_1/G_c have been performed in the framework of ANSYS-Fluent 14.0 computational fluid dynamics software. The detailed numerical procedure and methodology for the analysis of results are explained by Zambon.⁹ We only highlight here the main features of the procedure and additional numerical experiments performed for improving the final correlations for h_{wf} , h_{β} and G_1/G_c .

As described in ref 9, regular arrays of spherical particles between parallel plates were considered to this end. Heat exchange between the fluid and particles was suppressed by imposing zero thermal flux at the fluid–particle interfaces. Thus, the calculations were performed to quantify the heat exchange process between the flowing gas stream and the parallel plates maintained at uniform temperature. The regularity of the particle arrays allowed employing a basic cell with periodic boundary conditions. Consequently, asymptotic values of the parameters have been retrieved, without entry and exit effects.

The four regular arrays considered for calculations were those illustrated in Figure 6. They provide two levels of ε_1 , three levels of ε_c , and three levels of the difference ($\varepsilon_1 - \varepsilon_c$). The different combinations are significant for correlating the desired parameters.

Zambon⁹ assumed that the net direction of gas flow in the schemes in Figure 6 is vertical. However, the gas flow will face different particle configurations when the net direction is rotated around an axis normal to the plates, and heat exchange coefficients can be expected to change in this way. Therefore, further numerical experiments were carried out with the gas flow rotated 30° for hexagonal close packing (Hcp) and orthorhombic packing (Orp) and 45° for cubic close packing (Ccp) and simple cubic packing (Scp) (note that an additional turn with the same angle restores the same situation as for vertical flow). In particular, the results were significantly different for coefficient

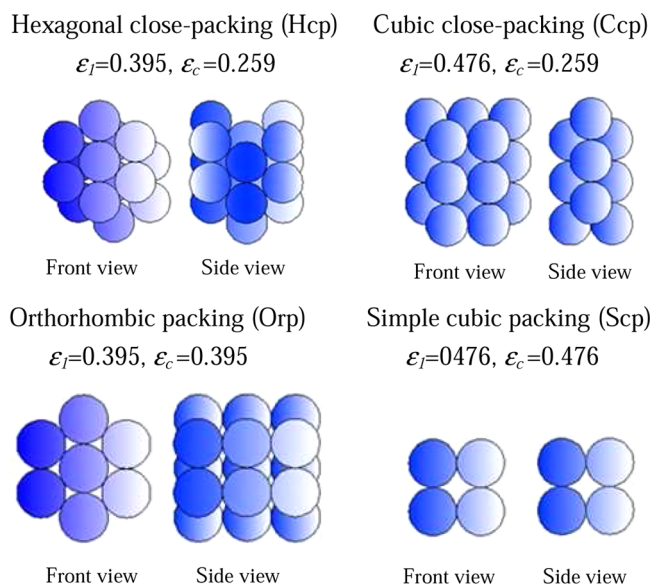


Figure 6. Regular arrays. “Front view” is parallel to the heat exchange plates.

h_{wf} in Hcp and Orp. The values employed for correlating h_{wf} , h_{β} and G_1/G_c were the averages from both configurations.

The number of layers between both plates was increased up to the point that no significant variations in the estimated values of the parameters h_{wf} , h_{β} and G_1/G_c arose for given operating conditions. In this way, seven layers were found to be suitable. Figure 7 shows the calculation cell for the Hcp.

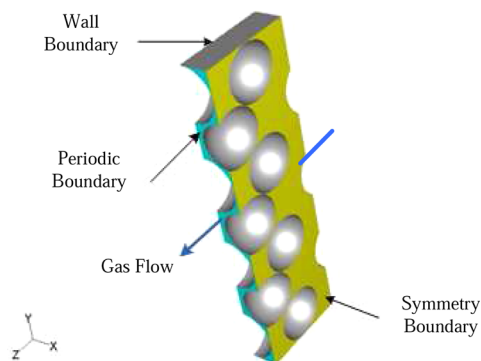


Figure 7. Cell with seven particle layers employed for CFD evaluation with Hcp.

To avoid a very fine meshing around particle–particle and particle–wall contact points, the diameter of the spheres was decreased by 1%. This procedure was found to be effective, as in previous works using it,^{29–31} and brought no significant lost of precision in the evaluation of the desired parameters.

The overall Reynolds number (based on overall superficial mass velocity G) in the range $100 < Re_p < 2000$ was considered by Zambon,⁹ while additional CFD experiments were performed for extending the range of Prandtl numbers: $0.4 < Pr < 3.5$. For values larger than $Re_p = 200$, the Spalart–Allmaras model of turbulence was employed.

The average heat flux at the wall (q_w) and mixing-cup temperature in the wall channel (T_1), within the calculation cell, were evaluated from the CFD results to estimate the wall heat transfer coefficient $h_{wf} = q_w / (T_1 - T_w)$. CFD velocity fields were

directly used to evaluate the ratio G_1/G_c . The 2R2D model proposed in section 3 was reformulated for a Cartesian transversal y -coordinate, no chemical reaction effect, and insulated particles. Given the values of q_w , T_1 , and G_1/G_c , values of h_f and $\lambda_{ef,c}$ were estimated by fitting the core channel temperature distribution of the model solution to the y -profile of the mixing-cup temperature from CFD calculations. As expected from the layered structure of the regular arrays, values of $\lambda_{ef,c}$ were lower than from correlations in random packed beds.

The values of $Nu_{wf} = h_{wf}D_p/\lambda_p$, $Nu_f = h_fD_p/\lambda_p$ and G_1/G_c were correlated with the bed structure parameters ε_1 and ε_c , Reynolds number, and Prandtl number, as summarized in Table 2.

Table 2. Correlations for Thermal and Fluid-Dynamic Parameters Obtained from CFD Temperature and Velocity Fields,⁹ with $100 < Re_p < 2000$ and $0.4 < Pr < 3.5$

$$\begin{aligned} Nu_{wf} &= A\varepsilon_1^\alpha Re_{p1}^\beta Pr^\gamma \\ A &= 0.285 \pm 0.008, \alpha = -2.4 \pm 0.4, \beta = 0.50 \pm 0.05, \gamma = 0.50 \pm 0.02 \\ Nu_f &= [A + B(\varepsilon_1 - \varepsilon_c)]\varepsilon_c^\alpha Re_p^\beta Pr^\gamma \\ A &= 0.34 \pm 0.03, B = 4 \pm 2, \alpha = 4.0 \pm 0.7 \\ G_1/G_c &= A\varepsilon_1^\alpha \varepsilon_c^\beta Re_p^\gamma \\ A &= 0.55 \pm 0.01, \alpha = 1.5 \pm 0.3, \beta = -2.4 \pm 0.2, \gamma = -0.04 \pm 0.03 \end{aligned}$$

Some aspects of the correlations in Table 2 are worth mentioning. Nu_{wf} is better correlated with wall channel parameters, ε_1 and $Re_{p1} = G_1D_p/\mu_p$, as expected. Also, note that the effects of Re_{p1} and Pr upon Nu_{wf} are of the form $(Re_{p1}Pr)^{0.5}$, just as in the well-known penetration theory. Instead, Nu_f depends directly on (Re_pPr) , revealing that the heat exchange mechanism between wall and core channels is dominated by convective effects, at least for $Re_p > 100$. The factor ε_1^α in the expression of Nu_f is most probably related to the size of the openings at $y^* = 1/2$. To explain the occurrence of the term $\varepsilon_1 - \varepsilon_c$, we can consider arrays with a symmetry plane at $y^* = 1/2$ (Orp and Scp in Figure 6). In this case $\varepsilon_1 - \varepsilon_c = 0$ and, accordingly, there will be a small driving force for convective exchange between both channels. On the contrary, $\varepsilon_1 > \varepsilon_c$ (Hcp and Ccp arrays in Figure 6) means that particles at the side of the first layer can be accommodated in its openings and the lower permeability at $y^* > 1/2$ can promote an incursion of the fluid from the core to the wall region and increase of Nu_f .

The effect of both void fractions ε_1 and ε_c on the ratio G_1/G_c is in the expected sense and Re_p shows only a modest influence.

Note that, using the analogy between heat and mass transfer, the correlation for Nu_f in Table 2 allows writing for the mass exchange coefficient between channels

$$a_f = h_f/(\delta_f c_{pf}) \quad (11)$$

To conclude this section, it should be said that the use of regular arrays allowed estimations of the parameters at significant different values of the structural properties ε_1 and ε_c , making it possible in this way to assess properly their effect. Nonetheless, as the final purpose is to evaluate h_{wf} , h_f and G_1/G_c in cylindrical random packed beds, the results presented here should ultimately be compared with evaluations in such conditions. Such evaluations are currently under way, and we expect that effects as those caused by the vessel curvature when $N \geq 5$ and defects in the structure of the first particle layer, such as those visualized in Figure 5, may be only of second order of magnitude.

5. COMPARISON BETWEEN THE PROPOSED 2R2D AND S2D MODELS FOR AN AMMONIA SYNTHESIS REACTOR

An ammonia synthesis reactor has been chosen as a basis to perform numerical evaluations employing the proposed 2R2D and S2D models. It should be noted that the goal in considering the ammonia synthesis process is not to carry out a rigorous simulation of the catalytic reactor, but to disclose some feature of the 2R2D model, and its comparison with the S2D model, under a realistic frame. Therefore, some aspects have been simplified or modified to gain a more clear interpretation of the results.

5.1. 2R2D Model. In order to assess in the 2R2D model the relevance of discriminating the thermal resistances at the wall ($1/h_{wf}$) and at the boundary between wall and core channels ($1/h_f$), the fluid radial exchange mechanisms will be assumed to dominate over conduction inside particles and between solid surfaces, a situation that in practice can hold at high enough values of Re_p . This assumption implies that local thermal equilibrium is achieved between particle and fluid. To maintain consistency, differences between C and C^* are also neglected. In this way, only the fluid conservation equations should be considered and the following formulation is derived from eqs 5a–9.

In the wall channel:

$$\begin{aligned} c_{pf}G_1 \frac{dT_1}{dz} &= (1 - \varepsilon_1)(-\Delta H)r_e(T_1, C_1) \\ &+ 2 \frac{\rho_t h_{wf}(T_w - T_1) + \rho_c h_f(T_{c,1} - T_1)}{\rho_t^2 - \rho_c^2} \end{aligned} \quad (12a)$$

$$G_1 \frac{d(C_1/\delta_f)}{dz} = (1 - \varepsilon_1)r_e(T_1, C_1) + 2 \frac{\rho_c \alpha_f(C_{c,1} - C_1)}{\rho_t^2 - \rho_c^2} \quad (12b)$$

In the core channel ($\rho < \rho_c$):

$$\begin{aligned} -\lambda_{ef,c} \frac{\partial(\rho \partial T_c / \partial \rho)}{\rho \partial \rho} + c_{pf}G_c \frac{\partial T_c}{\partial z} &= (1 - \varepsilon_c)(-\Delta H)r_e(T_c, C_c) \\ -D_{e,c} \frac{\partial(\rho \partial C_c / \partial \rho)}{\rho \partial \rho} + G_c \frac{\partial(C_c/\delta_f)}{\partial z} &= (1 - \varepsilon_c)r_e(T_c, C_c) \end{aligned} \quad (12c)$$

at $\rho = \rho_c$:

$$\begin{aligned} T_c &= T_{c,1}, \quad -\lambda_{ef,c} \frac{\partial T_c}{\partial \rho} = h_f(T_{c,1} - T_1) \\ C_c &= C_{c,1}, \quad -D_{e,c} \frac{\partial C_c}{\partial \rho} = \alpha_f(C_{c,1} - C_1) \end{aligned} \quad (12e)$$

5.2. S2D Model. For the S2D model, under the present assumptions, the following formulation applies.

$$-\lambda_{ef} \frac{\partial(\rho \partial T / \partial \rho)}{\rho \partial \rho} + c_{pf}G \frac{\partial T}{\partial z} = (1 - \varepsilon)(-\Delta H)r_e(C, T) \quad (13a)$$

$$-D_e \frac{\partial(\rho \partial C / \partial \rho)}{\rho \partial \rho} + G \frac{\partial(C/\delta_f)}{\partial z} = (1 - \varepsilon)r_e(C, T) \quad (13b)$$

Table 3. Base Set of Conditions and Properties Employed in the Simulations^a

operating conditions	thermophysical properties	tube and pellet dimensions
P [atm] = 300	δ_f [kg m ⁻³] = 49.05	H [m] = 3.00
T_w [K] = 650	c_{pf} [J kg ⁻¹ K ⁻¹] = 3356	D_t [m] = 0.04
G [kg m ⁻² s ⁻¹] = 0.786	μ_f [kg m ⁻¹ s ⁻¹] = 2.225×10^{-5}	D_p [m] = 0.008
($Re_p = 283$)	λ_f [W m ⁻¹ K ⁻¹] = 0.1858	($N = 5$)
	($Pr = 0.401$)	

^aInlet conditions: T_0 [K] = 650; N_2 [mol %] = 22.8; H_2 [mol %] = 67.7; NH_3 [mol %] = 5.4.

$$-\lambda_{ef} \frac{\partial T}{\partial \rho} = h_w(T_w - T), \quad \frac{\partial C}{\partial \rho} = 0, \quad \text{at } \rho = \rho_t/2 \quad (13c)$$

where G and ε are the overall superficial mass velocity and void fraction, which in terms of 2R2D values are evaluated as

$$G = [\rho_c^2 G_c + (\rho_t^2 - \rho_c^2) G_1] / \rho_t^2$$

$$\varepsilon = [\rho_c^2 \varepsilon_c + (\rho_t^2 - \rho_c^2) \varepsilon_1] / \rho_t^2$$

Average values will be suitable in section 5.3 to discuss differences between S2D and 2R2D models. The mixing-cup temperature in the core channel and in the whole cross section are expressed as

2R2D model:

$$\bar{T}_c = \frac{2 \int_0^{\rho_c} T_c \rho \, d\rho}{\rho_c^2}; \quad \bar{T} = \frac{\rho_c^2 G_c \bar{T}_c + (\rho_t^2 - \rho_c^2) G_1 T_1}{\rho_t^2 G}$$

S2D model:

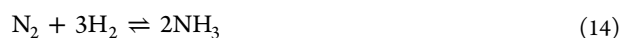
$$\bar{T} = \frac{2 \int_0^{\rho_t} T \rho \, d\rho}{\rho_t^2}$$

Similar definitions hold for mixing-cup concentrations.

In order to carry out a fair comparison between both models, the value of the wall heat transfer coefficient h_w of the S2D is evaluated by matching the behavior of the 2R2D model under two alternative reference conditions. One of them, leading to a value h_w^0 , is set by equating the asymptotic overall heat transfer coefficient from both models at constant T_w and without chemical reaction (i.e., by taking heat generation rate $Q \equiv (-\Delta H)r_c = 0$). The second one, giving h_w^Q , is defined in a similar way, but with a uniform value of Q . Both formulations are summarized in Appendix C.

To solve the 2R2D and S2D model formulations, discretization on the radial coordinate was done according to the Orthogonal Collocation Method,³² and the resulting set of algebraic and ordinary differential equations was integrated along the axial direction by using the STIFF3 algorithm³² modified by Barreto and Mazza.³³ For all cases discussed in section 5.4, the results using three or more collocation points were virtually the same. Compaq Visual Fortran 6.0 was used to perform the numerical solution.

5.3. Reaction Rate Expression, Operating Conditions, and Parameter Estimations.



is moderately exothermic [$(-\Delta H) = 111\,370$ J/mol has been used in the calculations], but reaction heat effects are potentially strong, as the N_2 and H_2 are almost stoichiometrically fed in the catalytic bed with only minor amounts of other species, e.g., NH_3 , from the recycle. Thus, the adiabatic temperature rise for

complete conversion is around 1000 K. Therefore, in some technologies the process is carried out in multitubular catalytic reactors, as will be assumed here.

The classical kinetic expression proposed by Temkin and Pyzhev³⁴ for Fe based catalysts will be employed here.

$$r_e \text{ [mol/(m}^3 \text{ s)}] = f \left(k \frac{p_{N_2} p_{H_2}^{1.5}}{p_{NH_3}} - k' \frac{p_{NH_3}}{p_{H_2}^{1.5}} \right) \quad (15)$$

$$k \left[\frac{\text{mol}}{\text{atm}^{1.5} \text{ m}^3 \text{ s}} \right] = 8280 \exp\left(-\frac{10475}{T \text{ [K]}}\right)$$

$$k' \left[\frac{\text{mol atm}^{0.5}}{\text{m}^3 \text{ s}} \right] = 11.9 \times 10^{15} \exp\left(-\frac{23871}{T \text{ [K]}}\right)$$

In eq 15 f is the catalyst activity factor, which is defined as explained later on.

In spite of the potentially large reaction-heat effects, ammonia synthesis reactors are not prone to suffer runaway, because the reverse reaction rate is strongly accelerated as temperature increases. In addition, as the molar ratio between N_2 and H_2 is nearly stoichiometric in the feed, the forward reaction rate rapidly diminishes when conversion increases. The effective forward reaction order is higher than 2.5, if the effect of $p_{NH_3}^{-1}$ is accounted for. Calculations considering the irreversible reaction rate from eq 15, i.e., taking $k' = 0$, will be also described.

The set of values used in the simulations is displayed in Table 3. Thermophysical properties were evaluated at the tube-inlet conditions and assumed constant along the tube. Results for inlet and wall temperatures different from 650 K will be also discussed. Nonetheless the thermophysical properties in Table 3 will be maintained.

The tube-to-particle diameter ratio in Table 3 is $N = 5$. As N is a key parameter to compare both models, simulations have been carried out at additional two levels, $N = 10, 20$. For this purpose, D_p was reduced and D_t was kept at the value reported in Table 3. However, in doing so the Reynolds number would decrease to $Re_p = 70$, a very low value for the comparison conditions stated at the beginning of section 5.1 and outside the range of the correlations presented in Table 2. Therefore, variations of N were accompanied by other two simultaneous changes. First, the mass flow velocity was raised to maintain $Re_p = 283$, i.e., G [kg m⁻² s⁻¹] = $0.786(N/5)$. In this way the residence time decreases causing temperature and conversion much lower than for $N = 5$. As this is undesirable to evaluate the effect of N , the activity factor f in eq 15 was also increased so as to maintain similar temperature levels. For $N = 5$ the activity factor is taken $f = 1$ and values for $N > 5$ will be informed in section 5.4.

To evaluate the structural parameters of the 2R2D model, $\eta_p^* = 1$ according to Mariani et al.,²⁵ $\varepsilon_c = 0.371 + 0.13/N$ (Mariani et al.³⁵), and the fraction ω from eq 1 were used. The correlation of

Table 4. Model Parameters (λ_{eff} W m⁻¹ K⁻¹; h_f W m⁻² K⁻¹)

N	2R2D model						S2D model			
	ε_1	ε_c	G_1/G_c	$\lambda_{\text{eff},c}$	h_f	h_{wf}	ε	λ_{eff}	h_w^0	h_w^Q
5	0.507	0.401	1.43	1.83	133	401	0.436	2.11	173	213
10	0.489	0.388	1.47	1.94	225	897	0.407	2.11	252	292
20	0.482	0.381	1.50	2.01	424	1942	0.391	2.11	420	484

Bey and Eigenberger³⁶ was employed to evaluate λ_{eff} and the random walk mechanism of Baron¹⁹ was used for D_c :

$$\lambda_{\text{eff}} = \frac{1}{10}(c_{\text{pf}}G)D_p \quad (16a)$$

$$D_c = \frac{1}{8}(G/\delta_f)D_p \quad (16b)$$

In using eqs 16a and 16b for the 2R2D model's parameters $\lambda_{\text{eff},c}$ and D_c , G_c instead of G is employed.

Expressions in Table 2 were employed for h_f , h_{wf} and G_1/G_c . eq 11 was used for α_f , while h_w was evaluated from the matching procedures explained in Appendix C.

5.4. Results and Discussion. The results for thermal parameters of 2R2D and S2D models are displayed in Table 4. Before presenting the results of the reactor simulations, some relevant observations from the values in Table 4 will be discussed next.

The ratio h_{wf}/h_f for the 2R2D model in Table 4 varies in the range $3 < h_{\text{wf}}/h_f < 4.5$, due to different values of ε_1 and ε_c as N changes. This range clearly reveals that the thermal resistance between channels is several times that at the wall. The ratio h_{wf}/h_f decreases at higher Re_p , but it can be checked from correlations in Table 2 or from the data in ref 9 that even at $Re_p = 2000$ the ratio h_{wf}/h_f keeps on being larger than 1. Then, the thermal resistance between channels will be larger than that at the wall for most commercial-scaled packed bed reactors.

The adjusted S2D coefficients h_w^0 and h_w^Q are closer to h_{wf} than to h_w . This can be expected in advance, as the thermal resistances $1/h_f$ and $1/h_{\text{wf}}$ of the 2R2D model operate in series and the former is much larger. However, $1/h_w^0$ and (especially) $1/h_w^Q$ are significantly lower than $1/h_f$ at $N = 5$, while some contribution of $1/h_{\text{wf}}$ might be expected. The finite (and significant for low N) extent of the wall channel promotes the relatively large matching values of h_w^0 and h_w^Q . This effect is weaker for $N = 20$ and h_w^0 becomes very close to h_f (Table 4). The corresponding Nusselt numbers show a significant effect of N , e.g., $Nu_w^0 = 7.5$ for $N = 5$ and $Nu_w^0 = 4.5$ for $N = 20$. On the other hand, differences between h_w^0 and h_w^Q are evident. Altogether, these observations emphasize the difficulty in assigning a clear physical meaning to the parameter h_w of the S2D model.

It is relevant to visualize the radial temperature profiles of both models. In Figure 8 the stationary profiles resulting for uniform heat generation $Q = 1700 \text{ kW m}^{-3}$ and $T_w = 650 \text{ K}$ are plotted for the 2R2D and S2D models, the latter with $h_w^Q = 213 \text{ W m}^{-2} \text{ K}^{-1}$ (Table 4). According to the fitting criterion, both profiles in Figure 8 present the same value $\bar{T} = 717.7 \text{ K}$ and the same flux at the wall ($q_w = 2Q/\rho_w$). In spite of the same value of \bar{T} , the variation of fluid temperature from the axis to the wall is significantly larger for the 2R2D model than for the S2D model. This is mainly so because the adjustment of the S2D model moves the effect of the large thermal resistance ($1/h_f$) between channels to the wall, where it does not exert influence on the fluid temperature. The same qualitative conclusion is reached when h_w^0 is used for the S2D model. If an exothermic catalytic reaction is

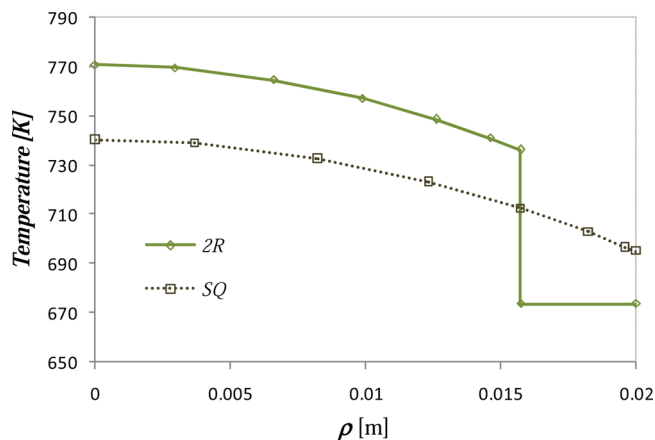


Figure 8. Stationary radial temperature profiles from 2R2D (2R) model and S2D model using h_w^Q (SQ), for $Q = 1700 \text{ kW m}^{-3}$ and $T_w = 650 \text{ K}$.

now assumed to take place under the temperature profiles in Figure 8, the average reaction rate will depend on the way that r_c depends upon T . If $\partial^2 r_c / \partial T^2 > 0$, as for an irreversible reaction, the larger variation of T around \bar{T} will usually make the average reaction rate from the 2R2D model be larger than that from the S2D model and a higher maximum of \bar{T} along the tube (hot spot) can be expected. Strongly reversible reactions, such as the ammonia synthesis reaction, can show $\partial^2 r_c / \partial T^2 < 0$ in practical ranges of temperature, and the hot spot temperature can be larger for the S2D model.

Other effects should also be mentioned as regards differences between values of \bar{T} predicted by both models. For example, the larger fraction of solids in the core region $[(1 - \varepsilon_c) > (1 - \varepsilon_1)]$ will tend to enlarge the difference discussed above. On the other hand, the reactant concentration in the core channel of the 2R2D model will be lower than in the corresponding zone of the S2D model, as the residence time is larger than in the wall channel ($G_c < G_1$) and an additional mass transfer resistance ($1/\alpha_f$) takes place at the boundary between channels. Although this effect plays an opposite role to those described above, it probably will not be determining for setting differences between both models, as mass transfer is usually fast enough to avoid significant radial concentration profiles.

Axial temperature and N_2 conversion profiles from the 2R2D model, corresponding to mixing-cup values in the core channel (\bar{T}_c and \bar{x}_c), in the whole cross section (\bar{T} and \bar{x}), and in the wall channel (T_1 and x_1), are presented in Figure 9 for the base case defined in Table 3. The axial positions (hot spots) where \bar{T}_c and \bar{T} show maximum values always are virtually coincident; therefore no distinction will be made in this respect henceforth. At the hot spot, maximum differences between temperatures (\bar{T}_c and T_1) and N_2 conversions (\bar{x}_c and x_1) in both channels also arise. The differences $\bar{T}_c - T_1$ and to a lesser degree $\bar{x}_c - x_1$ around the hot spot are very significant. The difference $\bar{x}_c - x_1$ responds to two causes: the different fluid velocities in wall and

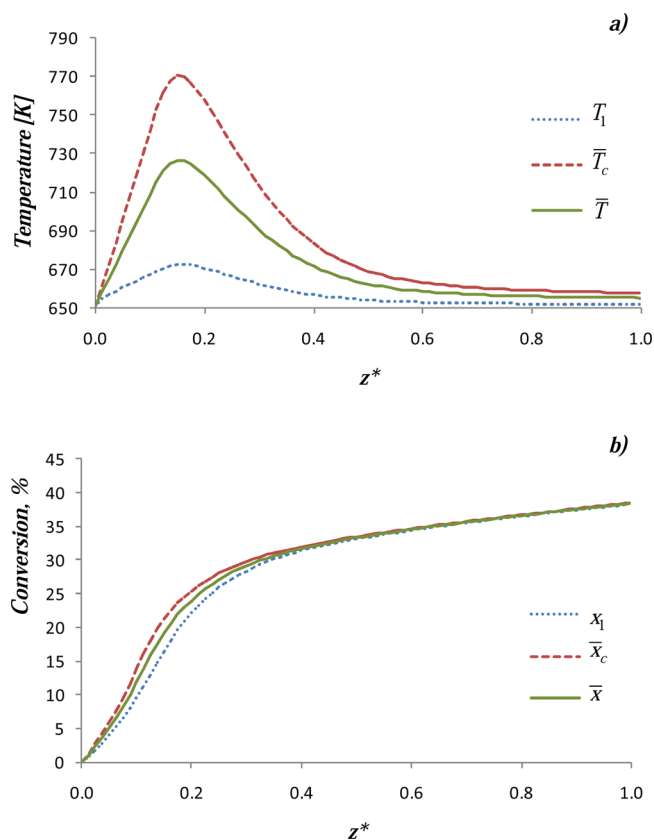


Figure 9. (a) Axial temperatures and (b) N_2 conversions from the 2R2D model. $T_0 = T_w = 650$ K, $N = 5$, r_e (eq 15) with $f = 1$.

core channels and the difference $\bar{T}_c - T_1$. The latter is far more relevant for most conditions in this study.

The effects of wall channel variables T_1 and x_1 on the averages \bar{T} and \bar{x} are very strong for the case $N = 5$ in Figure 9. This is not surprising, if we recall that the ratio between the cross-section area of the wall channel and the overall cross-section area is 36% and, taking into account the ratio G_1/G_c (Table 4), the mixing-cup contributions of the wall channel rise to almost 45%.

Also for the base case (Table 3), profiles of \bar{T} and \bar{x} from both models, 2R2D and S2D, are compared in Figure 10. 2R2D model's results are identified by the subscript "2R"; those from the S2D model with h_w^0 (no heat generation source, $Q = 0$) are identified by "S0" and those with h_w^Q (uniform Q) are identified by "SQ".

It can be appreciated in Figure 10a that hot spot values of \bar{T} from both models differ significantly. The differences between hot spot values $\bar{T}_{2R} - \bar{T}_{S0}$ and $\bar{T}_{2R} - \bar{T}_{SQ}$ nearly amount to 20 and 35%, respectively, of the temperature rise of the 2R2D model $\Delta\bar{T}_{2R} = \bar{T}_{2R} - T_w$. On the other hand, differences in N_2 conversion (Figure 10b) start to be significant around the hot spot and maintain relevance even up to the reactor exit ($z^* = 1$).

Radial temperature profiles at the hot spot predicted by each model in Figure 10a are plotted in Figure 11a. The companion conversion radial profiles are presented in Figure 11b.

Modest changes in conversion are observed from the 2R2D model in Figure 11b, mainly due to the mass transfer resistance $1/\alpha_f$ between the channels, while negligible variations are predicted by the S2D model. These observations are valid for all cases discussed in this section.

The radial temperature profiles in Figure 11a show that the maximum axis temperature (T^{ax}) predicted by the models are

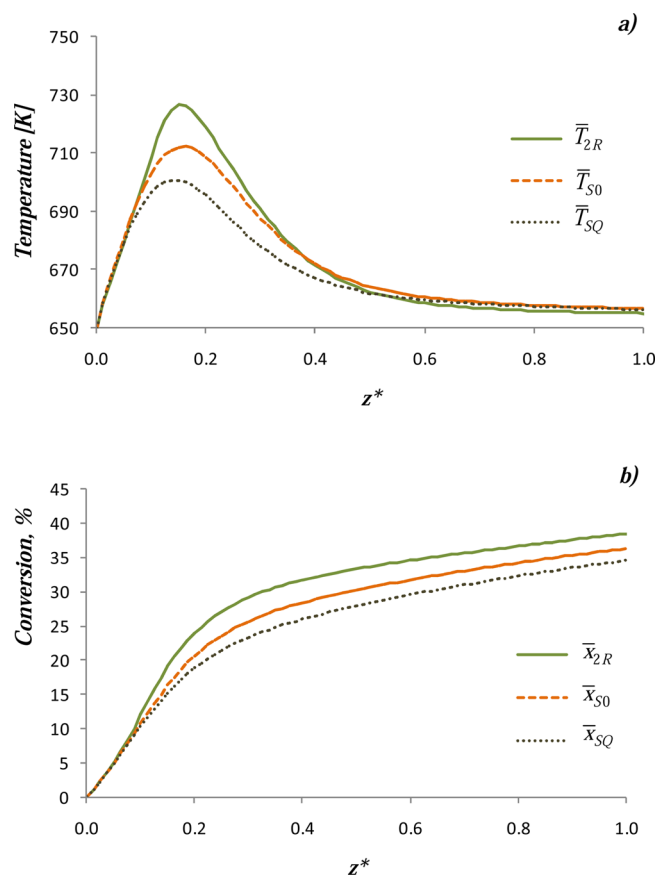


Figure 10. Profiles of (a) \bar{T} and (b) \bar{x} predicted by 2R2D and S2D models. $T_0 = T_w = 650$ K, $N = 5$, r_e (eq 15) with $f = 1$.

very different. This feature is important, as T^{ax} defines the highest thermal level in the bed and therefore its correct prediction is paramount to checking tolerable temperature limits. For example, the difference $T_{2R}^{\text{ax}} - T_{SQ}^{\text{ax}} = 71.7$ K in Figure 11a is very significant as it represents 50% of the temperature rise in the axis predicted by the 2R2D model ($T_{2R}^{\text{ax}} - T_w = 142.5$ K).

It was discussed before in this section that the sign of $\partial^2 r_e / \partial T^2$ can be expected to determine which model will predict the highest value of \bar{T} along the tube. In the case illustrated in Figures 10 and 11, the fields of temperature and concentration involved in the S2D model from the bed inlet up to the hot spot are such that always $\partial^2 r_e / \partial T^2 > 0$. Nearly the same happens from the results of the 2R2D model, although approaching the hot spot the sign of $\partial^2 r_e / \partial T^2$ changes along the radial variable (in Figure 11a $\partial^2 r_e / \partial T^2 > 0$ in the wall channel, but $\partial^2 r_e / \partial T^2 < 0$ in almost the whole core channel). As a result, the maximum value of \bar{T} is predicted by the 2R2D model.

This analysis suggests that, if $T_0 = T_w$ is raised up to a certain value, the maximum \bar{T} will be found from the S2D model, as the acceleration of the reverse reaction (see eq 15) will make the sign of $\partial^2 r_e / \partial T^2$ become negative in an earlier stage during the rise of temperature along the bed. In Figure 12, temperature and conversion axial profiles are plotted for the same conditions as in Figure 10, but with $T_0 = T_w = 700$ K. In agreement with expectations, higher hot-spot values of \bar{T} are predicted by the S2D model (either using h_w^0 or h_w^Q). Further increases of $T_0 = T_w$ up to around 800 K do not significantly modify either the magnitude or the sign of the differences between models. In the end ($T_0 = T_w > 850$ K), a very low equilibrium conversion is rapidly reached close to the bed inlet. It can be concluded that a

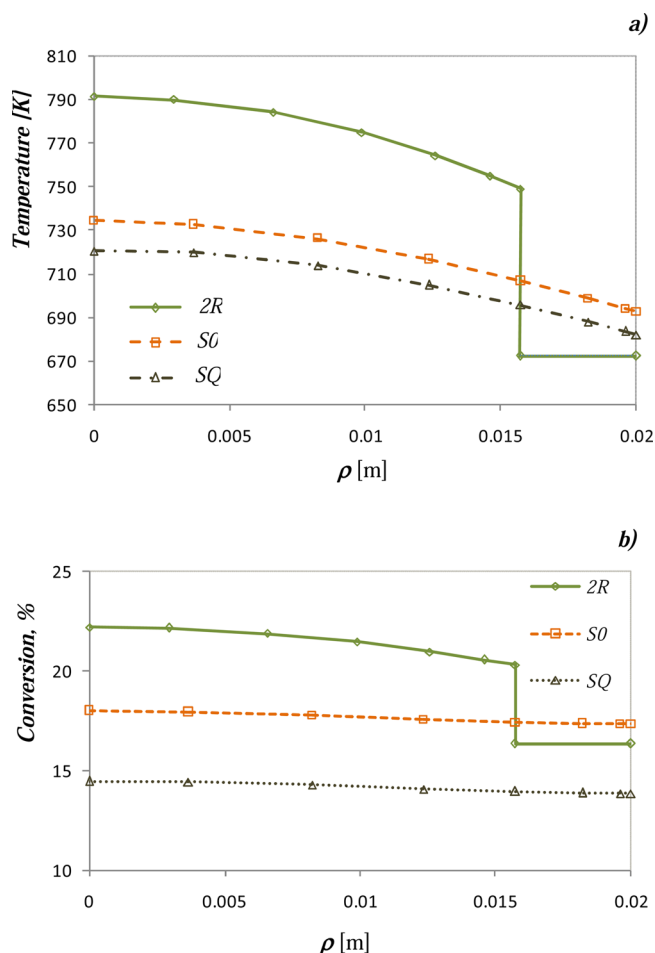


Figure 11. (a) Radial temperature and (b) N_2 conversion profiles predicted by 2R2D and S2D models at the hot spot. $T_0 = T_w = 650$ K, $N = 5$, r_e (eq 15) with $f = 1$.

strongly reversible reaction such as the one treated here moderates the effect of temperature, and phenomena described as “reactor runaway” or “reaction ignition” can be hardly identified. As a consequence, differences between models are also tempered.

It is therefore important to explore differences between models for the case of exothermic irreversible reactions, such as are very common in many other industrial multitubular reactors (e.g., hydrocarbon partial oxidations or oxy-dehydrogenations). To avoid changing the whole platform of calculation, we will simply consider the same case presented in section 5.3, but dropping the reverse reaction rate in eq 15. Values of properties (Table 3) and parameters (Table 4) will be maintained. Also, the adiabatic temperature rise using $(-\Delta H) = 111\,370$ J/mol and activation energy in eq 15 are well in the range of those found, e.g., for partial oxidation reactions.

As $\partial^2 r_e / \partial T^2 > 0$ is guaranteed by an irreversible reaction, the first evaluation with the irreversible reaction is to check if at $T_0 = T_w = 700$ K the sign of the differences between hot spot values $\bar{T}_{2R} - \bar{T}_{S0}$ and $\bar{T}_{2R} - \bar{T}_{SQ}$ change with respect to the reversible case in Figure 12a. To do this, however, the activity factor f (see eq 15) has to be lowered; otherwise the hypothetical irreversible reaction ignites (even below $T_0 = T_w = 700$ K) and the temperature rises to very high levels (~ 1500 K). The value $f = 0.4$ leads to maximum values \bar{T} similar to those of the reversible case in Figure 12a (around 800 K). The profiles of \bar{T} and \bar{x} thus

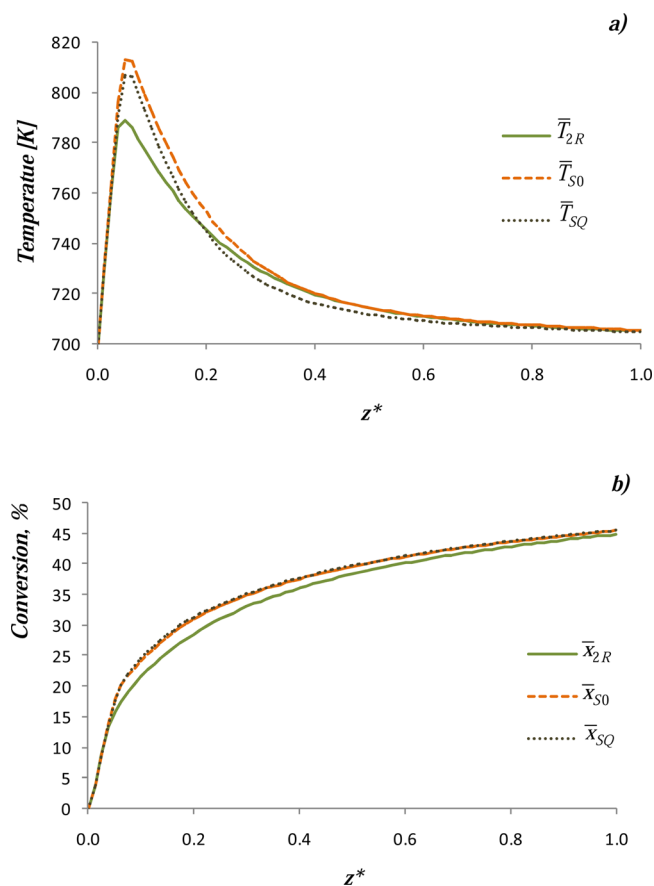


Figure 12. Profiles of (a) \bar{T} and (b) \bar{x} predicted by 2R2D and S2D models. $T_0 = T_w = 700$ K, $N = 5$, r_e (eq 15) with $f = 1$.

obtained are displayed in Figure 13. The 2R2D model effectively predicts higher temperatures, and the magnitude of the differences with the S2D model’s predictions are quite large. The hot spot values $\bar{T}_{S0} - T_w$ and $\bar{T}_{SQ} - T_w$ only reach 50% of the 2R2D model’s value $\bar{T}_{2R} - T_w$. Conversions predicted from both models are also significantly different: values from the S2D model are around 25% lower than those from the 2R2D model at the bed exit.

In practice, the difference between models seems to be governed by the ability to predict average reaction rates, which in turn has been related to $\partial^2 r_e / \partial T^2$. The magnitude of the effect will be more properly quantified by the product $(\partial^2 r_e / \partial T^2)(\bar{T} - T_w)^2 / r_e$, with $\bar{T} - T_w$ evaluated at the hot spot and $(\partial^2 r_e / \partial T^2) / r_e$ at some appropriate position between the bed inlet and the hot spot. If $\bar{T} - T_w$ is low enough, the models should predict very similar temperature rises if h_w has been correctly evaluated. As an example, the same (irreversible) case as in Figure 13, but with $T_0 = T_w = 650$ K, leads to a maximum temperature rise $\bar{T}_{2R} - \bar{T}_w \approx 18$ K and the corresponding values of the S2D model (with either h_w^0 or h_w^Q) only differ in about ± 1 K. Other conditions involving low enough values of $\bar{T} - T_w$ are always accompanied by negligible differences between the models, showing that values of h_w^0 or h_w^Q chosen for the comparison are indeed suitable.

The effect of changing the aspect ratio N will be now discussed for the base case (Figures 9–11) and for the irreversible case at $T_0 = T_w = 700$ K (Figure 13). We recall that parameter values are those in Table 4. The catalytic activity factor f has been changed with N so as to keep the same hot spot value \bar{T}_{2R} that arises when $N = 5$. The results of average temperatures \bar{T} and axis

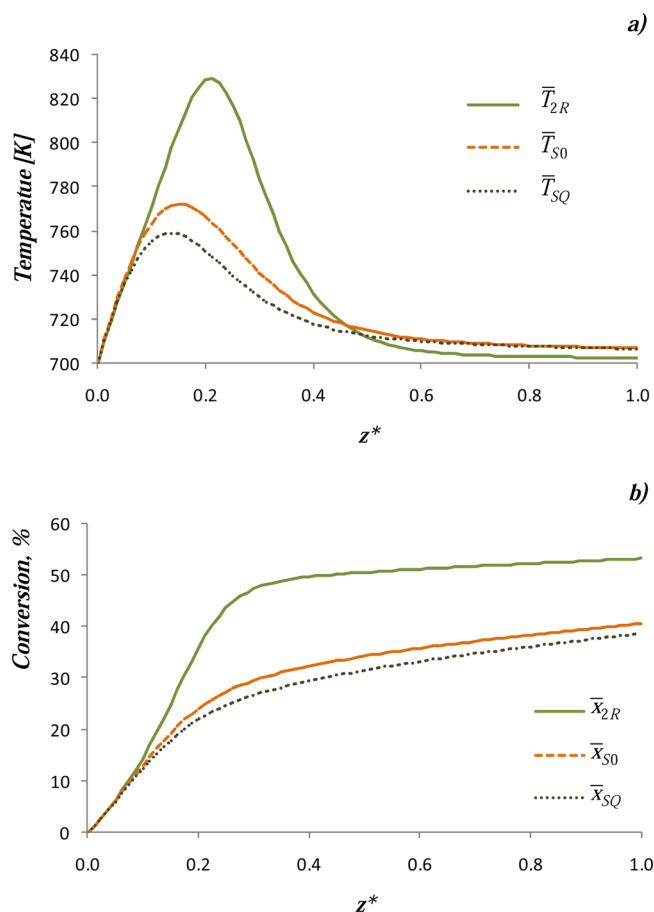


Figure 13. Profiles of (a) \bar{T} and (b) \bar{x} predicted by 2R2D and S2D models. $T_0 = T_w = 700$ K, $N = 5$, r_e (eq 15) with $k' = 0$ (irreversible case) and $f = 0.4$.

temperatures T^{ax} in the hot spots and average conversions \bar{x} at the bed exit are presented in Tables 5 and 6. To better appraise the significance of differences between the models, average temperatures from the S2D models are expressed by the ratios

$$\bar{R}_{S0}\% = 100 \left(\frac{\bar{T}_{2R} - \bar{T}_{S0}}{\bar{T}_{2R} - T_w} \right), \quad \bar{R}_{SQ}\% = 100 \left(\frac{\bar{T}_{2R} - \bar{T}_{SQ}}{\bar{T}_{2R} - T_w} \right) \quad (17a)$$

and for the axis temperatures

$$R_{S0}^{\text{ax}}\% = 100 \left(\frac{T_{2R}^{\text{ax}} - T_{S0}^{\text{ax}}}{T_{2R}^{\text{ax}} - T_w} \right), \quad R_{SQ}^{\text{ax}}\% = 100 \left(\frac{T_{2R}^{\text{ax}} - T_{SQ}^{\text{ax}}}{T_{2R}^{\text{ax}} - T_w} \right) \quad (17b)$$

For the base case (Table 5), significant differences between temperatures predicted by the models are found up to $N = 10$, with axis values $R_{S0}^{\text{ax}}\%$ and $R_{SQ}^{\text{ax}}\%$ being always more important.

Table 5. Average and Axis Temperatures at the Hot Spot and Average Exit Conversions^a

N	f	$\bar{T}_{2R} - T_w$	$\bar{R}_{S0}\%$	$\bar{R}_{SQ}\%$	$T_{2R}^{\text{ax}} - T_w$	$R_{S0}^{\text{ax}}\%$	$R_{SQ}^{\text{ax}}\%$	$\bar{x}_{2R}\%$	$(\bar{x}_{2R} - \bar{x}_{S0})\%$	$(\bar{x}_{2R} - \bar{x}_{SQ})\%$
5	1.0	76.4	18.6	33.6	142.5	40.9	49.9	38.4	2.10	3.80
10	1.25	76.6	13.3	23.9	132.8	25.9	33.1	35.4	2.06	3.49
20	1.68	76.5	3.1	11.9	137.8	10.7	16.0	32.6	0.75	1.86

^aRatios R_{S0} and R_{SQ} defined in eqs 17a and 17b. $T_0 = T_w = 650$ K; r_e (eq 15).

For $N = 20$, already a large ratio for multitubular industrial reactors, the differences can be regarded as being almost negligible for practical purposes. On the other hand, exit conversions show low differences, even at $N = 5$.

When the reverse reaction is suppressed (Table 6), thermal levels predicted by the models keep on being significantly different even at $N = 20$. The behavior of exit conversions is markedly different from the reversible case, with notorious differences also up to $N = 20$.

The results presented in this section suggest that the intrinsic difference in the thermal descriptions of the 2R2D and S2D models would be reflected in the accuracy of their predictions for a variety of practical cases.

6. CONCLUSIONS

A two-dimensional (2D) model aimed at improving the heat transfer description of multitubular packed-bed catalytic reactors has been introduced in this paper. At present, the model is restricted to spherical packing. The model, named the two-region two-dimensional (2R2D) model, identifies the different effects concentrated in the wall thermal resistance ($1/h_w$) of the so-called standard 2D model (S2D) and locates them in accordance with the highly ordered packing close to the vessel walls. In this sense, a fluid channel from the wall up to a distance $D_p/2$ and a particle layer against the wall are identified. Formulation of the model is given in section 3.2, but the alternative developed in Appendix A is strongly suggested for practical numerical implementation. The thermal and structural parameters introduced by the model have been analyzed, and it is concluded that most of them correspond to effective properties that have been already evaluated in the literature or can be estimated from them (see Appendix B). On the other hand, the thermal exchange coefficient between wall and core channels h_f and the “true” wall–fluid heat transfer coefficient h_{wf} need further evaluation. These parameters, along with the ratio of mass velocity in the wall channel and in the remainder of the bed (core channel) G_1/G_c have been recently evaluated by using a CFD technique in beds of regular arrays of spheres and the results expressed in terms of correlations with the bed structure parameters and operating conditions. As expected from the conceptual description of the model, the thermal resistance between channels $1/h_f$ is substantially larger than that of the true film resistance at the wall $1/h_{wf}$ up to Reynolds numbers as large as ~ 2000 .

To assess differences between the descriptions provided by the proposed 2R2D model and the S2D model, a multitubular packed-bed catalytic reactor intended for ammonia synthesis was employed as a base case for the simulations. To emphasize the discrimination between thermal resistances $1/h_{wf}$ and $1/h_f$ the fluid radial exchange mechanisms were assumed to dominate over conduction inside particles and between solid surfaces, a situation that in practice can hold at high enough values of Re_p .

The overall heat exchange capacities of both models were matched by adjusting the S2D model’s parameter h_w , using two

Table 6. Average and Axis Temperatures at the Hot Spot and Average Exit Conversions^a

N	f	$\bar{T}_{2R} - T_w$	$\bar{R}_{S0}\%$	$\bar{R}_{SQ}\%$	$T_{2R}^{ax} - T_w$	$R_{S0}^{ax}\%$	$R_{SQ}^{ax}\%$	$\bar{x}_{2R}\%$	$(\bar{x}_{2R} - \bar{x}_{S0})\%$	$(\bar{x}_{2R} - \bar{x}_{SQ})\%$
5	0.40	128.3	43.0	53.9	253.2	61.2	67.1	53.2	12.6	14.6
10	0.535	128.2	31.7	40.9	237.8	44.4	50.7	50.7	10.3	12.6
20	0.714	128.5	18.8	28.8	256.1	28.1	35.9	49.1	6.92	9.80

^aRatios R_{S0} and R_{SQ} defined in eqs 17a and 17b. $T_0 = T_w = 700$ K; r_e (eq 15) with $k' = 0$ (irreversible case).

alternative criteria (Appendix C). Values of h_w are related to h_f but no clear physical meaning could be assigned to them.

Comparison between the 2R2D and S2D models was performed under two kinetic schemes: the actual reversible reaction rate for ammonia synthesis (reversible case) and the irreversible reaction rate that results by ignoring the reverse reaction (irreversible case). The latter was undertaken to simulate important applications involving irreversible reactions, such as hydrocarbon partial oxidations, and also to disclose specific features shown by severely equilibrium limited reactions, such as ammonia synthesis.

Differences between both models have been discussed mainly in terms of different temperatures predicted at the hot spot. The analysis of the features of both models and numerical results allowed concluding that the main cause of temperature differences is the large thermal resistance $1/h_f$ between channels of the 2R2D model. At a given aspect ratio N , the magnitude of the differences is determined by the product $(\partial^2 r_e / \partial T^2)(\bar{T} - T_w)^2 / r_e$, where $\bar{T} - T_w$ is evaluated at the hot spot by, e.g., the 2R2D model, and $(\partial^2 r_e / \partial T^2) / r_e$ is evaluated at some appropriate position between the bed inlet and the hot spot. Whether the 2R2D model will predict a higher or lower value of hot spot temperature is defined by the sign of $\partial^2 r_e / \partial T^2$. The second derivative is always positive for an irreversible reaction, and temperatures from the 2R2D model are always higher. Also, the high parametric sensitivity and reaction ignition phenomena shown by irreversible reactions are associated with strictly positive values of $\partial^2 r_e / \partial T^2$. Then, the numerical comparison of the 2R2D and S2D models for the irreversible case showed that predicted average and axis temperatures at the hot spot are likely to be much different under reasonable operating conditions and monotonically increase as the reference temperatures $T_0 = T_w$ are raised, up to the point of reaction ignition. Exit conversions also differ significantly. Differences between models remain large in the range of aspect ratios $5 < N < 10$, and decay significantly only when $N = 20$.

The behavior of the reversible case (analyzed with the original ammonia synthesis reaction rate) is rather different. The sign of differences between temperatures at the hot spot predicted by both models changes when the reference temperatures $T_0 = T_w$ reach some specific value, as a consequence of the change in sign of $\partial^2 r_e / \partial T^2$. Further increase in $T_0 = T_w$ does not modify much the magnitude of the differences between models. Although in the reversible case temperature rises above $T_0 = T_w$ are moderate, significant differences from both models in hot spot average and axis temperatures are still found at $N = 5$. Nonetheless, the effect of N is stronger than in the irreversible case: at $N = 10$ the differences between models decrease significantly and almost disappear at $N = 20$.

Further investigation on coefficients h_f and h_{wf} in random packed beds of spheres are under way. The next stage in our planning is the assemblage of new and old parameters to obtain a reliable set for modeling catalytic packed bed reactors. A relevant additional issue concerns the effect of packing shapes different from spherical. In particular, cylindrical particles deserve due

consideration, as they are commonly employed. In this regard, it is expected that the conceptual description of the 2R2D model can be maintained, but evaluation of certain parameters here undertaken should be revised, namely the location of the boundary between wall and core channels and correlations (Table 2) for h_f , h_{wf} and G_1/G_c .

APPENDIX A: REFORMULATION OF PROPOSED 2R2D MODEL BY INTRODUCING OUTER AND INNER CORE CHANNELS

To make equal the sizes of core regions for the fluid and solid, a lumped description can be adopted for the fluid in the zone $1/2 < y^* < y_L^*$, which will be identified as the *outer core channel*. In terms of the radial variable, this zone extends over $\rho_L < \rho < \rho_o$, its thickness is $\rho_c - \rho_L = D_p(y_L^* - 1/2)$, and its temperature and concentration levels are defined by T_2 and C_2 , respectively. The *inner core channel* extends over $0 < \rho < \rho_L$, i.e., matching the size of the solid core region.

The sketch in Figure 3 becomes modified according to Figure 14. The radial thermal resistance of the outer core channel is split

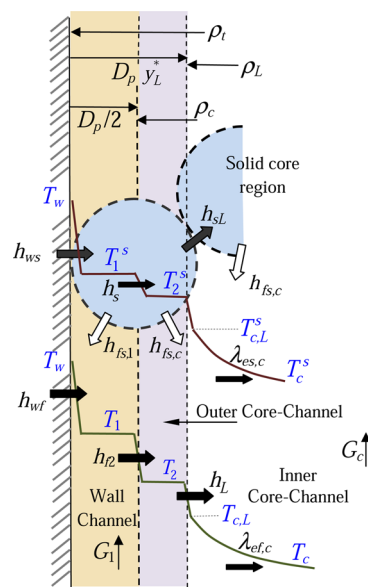


Figure 14. Modified sketch for the 2R2D model (see Figure 3 in the main text) introducing an outer core channel ($\rho_L < \rho < \rho_c$) and an inner core channel ($0 < \rho < \rho_L$).

and each half is concentrated at the boundaries with the wall channel and the inner core channel. Thus, at the boundary with the wall channel the heat exchange coefficient h_f is corrected according to

$$h_{f2} = \left[\frac{1}{h_f} + \rho_c \frac{\ln(\rho_c / \rho_L)}{2\lambda_{ef,c}} \right]^{-1} \quad (\text{A1a})$$

and the heat exchange coefficient h_L between the outer and inner core channels becomes expressed as

$$h_L = \frac{1}{\rho_L} \frac{2\lambda_{ef,c}}{\ln(\rho_c/\rho_L)} \quad (\text{A1b})$$

The analogous mass exchange coefficients α_{f2} and α_L are obtained from eqs A1a and A1b by using α_f instead of h_f and $D_{e,c}$ instead of $\lambda_{ef,c}$.

Conservation equations for the first particle layer and solid core regions remain the same as in the text (eqs 6a, 6b, 8a, and 8b), while for the fluid in the wall and core channels the formulation becomes (from eqs 5a, 5b, and 7a–7d in the text) the following.

In the *wall channel* ($\rho_c < \rho < \rho_i$):

$$c_{pf}G_1 \frac{dT_1}{dz} = (1 - \varepsilon_1) \frac{6h_{fs,1}}{D_p} (T_1^s - T_1) + \frac{2\rho_t h_{wf}(T_w - T_1) + 2\rho_c h_{f2}(T_2 - T_1)}{\rho_t^2 - \rho_c^2} \quad (\text{A2a})$$

$$G_1 \frac{d(C_1/\delta_f)}{dz} = (1 - \varepsilon_1) \frac{6\alpha_{fs,1}}{D_p} (C_1^s - C_1) + \frac{2\rho_c \alpha_{f2}(C_2 - C_1)}{\rho_t^2 - \rho_c^2} \quad (\text{A2b})$$

In the *outer core channel* ($\rho_L < \rho < \rho_c$):

$$c_{pf}G_c \frac{dT_2}{dz} = (1 - \varepsilon_c) \frac{6h_{fs,c}}{D_p} (T_2^s - T_2) + \frac{2\rho_L h_L(T_{c,L} - T_2) + 2\rho_c h_{f2}(T_1 - T_2)}{\rho_c^2 - \rho_L^2} \quad (\text{A3a})$$

$$G_c \frac{d(C_2/\delta_f)}{dz} = (1 - \varepsilon_c) \frac{6\alpha_{fs,c}}{D_p} (C_2^s - C_2) + \frac{2\rho_L \alpha_L(C_{c,L} - C_2) + 2\rho_c \alpha_{f2}(C_1 - C_2)}{\rho_c^2 - \rho_L^2} \quad (\text{A3b})$$

In the *inner core channel* ($\rho < \rho_L$):

$$-\lambda_{ef,c} \frac{\partial(\rho \partial T_c / \partial \rho)}{\rho \partial \rho} + c_{pf}G_c \frac{\partial T_c}{\partial z} = (1 - \varepsilon_c) \frac{6h_{fs,c}}{D_p} (T^s - T_c) \quad (\text{A4a})$$

$$-D_{e,c} \frac{\partial(\rho \partial C_c / \partial \rho)}{\rho \partial \rho} + G_c \frac{\partial(C_c/\delta_f)}{\partial z} = (1 - \varepsilon_c) \frac{6\alpha_{fs,c}}{D_p} (C^s - C_c) \quad (\text{A4b})$$

at $\rho = \rho_L$:

$$T_c = T_{c,L}, \quad -\lambda_{ef,c} \frac{\partial T_c}{\partial \rho} = h_L(T_{c,L} - T_2) \quad (\text{A4c})$$

$$C_c = C_{c,L}, \quad -D_{e,c} \frac{\partial C_c}{\partial \rho} = \alpha_L(C_{c,L} - C_2)$$

It is remarked that the modification presented in this appendix does not introduce any new thermal or mass transfer parameters, as the coefficients h_{f2} and h_L in eqs A1a and A1b only depend on parameters already defined, and a similar observation holds for α_{f2} and α_L .

■ APPENDIX B: HEAT TRANSFER IN THE FIRST PARTICLE LAYER. EVALUATION OF COEFFICIENTS h_s , h_{ws} , AND h_{sL}

In order to evaluate coefficient h_s , we will consider for the first particle layer a reference case defined by $N \rightarrow \infty$ ($\omega = 1/2$), negligible reaction heat effect, and negligible heat exchange with the wall surface and with the core-region particles. This situation could correspond to high Re_p numbers, when convective heat exchange with the fluid will determine the thermal behavior of the first particle layer. It is further assumed that $h_{fs,1} = h_{fs,c} \equiv h_{fs}$. Taking into account eqs 2a–4b in the main text, under the conditions defined above eqs 6a and 6b are reduced as follows:

$$\frac{\pi}{2} n_p^* h_{fs} (T_1^s - T_1) + h_s (T_1^s - T_2^s) = 0 \quad (\text{B1a})$$

$$\frac{\pi}{2} n_p^* h_{fs} (T_2^s - T_2) + h_s (T_2^s - T_1^s) = 0 \quad (\text{B1b})$$

The fluid temperature is assumed to show a linear variation with the coordinate y^* (normal to the wall surface):

$$T = (T_1 + T_2)/2 + (y^* - 1/2)(T_2 - T_1), \quad 0 < y^* < 1 \quad (\text{B2})$$

where T_1 and T_2 are average temperatures in the wall channel ($0 < y^* < 1/2$) and in the part of the core-channel zone defined by $1/2 < y^* < 1$, respectively. The energy balance within a given spherical particle is simply stated as

$$\nabla^2 \theta = 0 \quad \text{in } V_p \quad (\text{B3a})$$

$$-\lambda_p \nabla_n \theta = h_{fs}(\theta - T) \quad \text{on } S_p \quad (\text{B3b})$$

where ∇_n is the projection of the gradient on the normal to the external surface, θ is the local particle temperature, and λ_p is the particle thermal conductivity.

The solution of the problem (eqs B2, B3a, and B3b) for θ can be written as

$$\theta = (T_1 + T_2)/2 + \frac{Bi_{fs}}{1 + Bi_{fs}/2} (y^* - 1/2)(T_2 - T_1) \quad (\text{B4})$$

where $Bi_{fs} = h_{fs} D_p / \lambda_p$ is the Biot number.

It is noted that the dependence of θ just on coordinate y^* is not a simplification, but a feature arising from the type of boundary condition in this problem (i.e., as defined by eqs B2 and B3b).

From eq B4, the following is obtained for the surface average temperature on the hemispheres at each side of $y^* = 1/2$:

$$T_1^s = (T_1 + T_2)/2 - \frac{Bi_{fs}}{1 + Bi_{fs}/2} (T_2 - T_1)/4$$

$$T_2^s = (T_1 + T_2)/2 + \frac{Bi_{fs}}{1 + Bi_{fs}/2} (T_2 - T_1)/4$$

By replacing T_1^s and T_2^s in either eq B1a or eq B1b, the following is obtained for h_s :

$$h_s = \frac{\pi}{2} n_p^* \lambda_p / D_p \quad (\text{B5a})$$

The coefficient h_s^1 based on the projected particle area $\pi D_p^2/4$ (area of the intersection between a particle and a plane at $y^* = 1/2$) is related to h_s as

$$h_s = \frac{\pi}{4} n_p^* h_s^1 \quad (\text{B5b})$$

Consequently

$$h_s^1 = \lambda_p / (D_p/2) \quad (\text{B5c})$$

Equation B5c clearly expresses that the thermal resistance inside the particle is equivalent to that of a cylinder of diameter D_p and length $D_p/2$.

As explained in the main text, the proposed model is expected to be suitable when relatively low values of $T_1^s - T_2^s$ arise. In this case, the results will not be sensitive to values of h_s and therefore refinements to eqs B5a–B5c probably will not be necessary.

Turning back to eqs 6a and 6b in the main text, it is remarked that the driving forces for coefficients h_{ws} and h_{sL} are based on the surface average temperatures at each side of the particle, T_1^s and T_2^s , respectively. Literature references (e.g., ref 14) define similar coefficients, here denoted h_{wp} and h_{pL} , but with driving forces based on an overall particle temperature, which will be denoted T^s . Therefore, coefficient h_{ws} should be smaller than h_{wp} by virtue of their respective driving forces: $T_1^s - T_w$ and $T^s - T_w$, respectively. A similar comment applies for the pair h_{sL} and h_{pL} , defined with driving forces $T_2^s - T_{c,L}^s$ and $T^s - T_{c,L}^s$, respectively.

To establish the relationships between each pair of related coefficients, consider the first particle layer exchanging heat just with the wall and with adjacent particles, i.e., under negligible reaction heat effect and no heat exchange with the fluid (a situation likely to apply at low Re_p). Thus, the heat flux at the wall (ρ_t) can be expressed as

$$q_w = \frac{\rho_L h_{pL} h_{wp}}{\rho_L h_{pL} + \rho_t h_{wp}} (T_{c,L}^s - T_w) \quad (\text{B6})$$

Using eqs 6a and 6b in the text in the same situation (i.e., neglecting the reaction heat and particle/fluid exchange terms), eq B6 can be exactly satisfied by defining

$$\frac{1}{h_{ws}} = \frac{1}{h_{wp}} - \frac{\rho_t}{2\rho_c h_s} \quad (\text{B7a})$$

$$\frac{1}{h_{sL}} = \frac{1}{h_{pL}} - \frac{\rho_L}{2\rho_c h_s} \quad (\text{B7b})$$

There are expressions available in the literature to estimate the heat transfer coefficient h_{wp} , e.g., as given by Legawiec and Ziółkowski.²⁴ These authors developed the expression of h_{wp} by considering the curvature of the wall surface and assuming flux lines in the direction of the radial coordinate. Although the flux-line assumption may not be suitable for highly conductive solids, it seems a reasonable simplification for many catalyst materials.

As each particle in the first layer will share more than one contact point with adjacent particles, it is expected that h_{pL} can be related to the effective particle-to-particle thermal conductivity $\lambda_{es,c}$ which can be estimated from, e.g., the correlation analyzed by Bauer and Schlünder.²⁸ Assuming the bed as a set of successive layers of particles separated by a distance $L = D_p(2y_L^* - 1)$, as expressed in section 3.1, the relationship between h_{pL} and $\lambda_{es,c}$ can be written as

$$h_{pL} = 2\lambda_{es,c}/L = 2\lambda_{es,c}/[D_p(2y_L^* - 1)] \quad (\text{B8})$$

For finite values of N , curvature effects may introduce some uncertainty about the suitable surface of reference for h_{pL} given by eq B8. The following reasoning leads to the conclusion that the suitable surface is that at $\rho = \rho_L$ (at $y^* = y_L^*$, see Figure 3), i.e., the surface used as reference for h_{sL} in the main text. Since $\lambda_{es,c}$ is assumed constant in the solid core region of the proposed 2R2D model, and considering that the main thermal resistance quantified by $1/\lambda_{es,c}$ is that around contact points, the energy conservation balance in the solid core region (eq 8a) implicitly assumes that at any radial position the number of contact points is proportional to the perimeter $2\pi\rho$. If this description is applied to the boundary between the first particle layer and the solid core region, where the contact points can be identified at $y^* = y_L^*$, the relation between $\lambda_{es,c}$ and h_{pL} , as given by eq B8, is appropriately assigned to hold at $y^* = y_L^*$ (rather than, e.g., at $y^* = 1/2$).

Equations B5a–B5c, B7a, B7b, and B8 are the main results from this appendix.

■ APPENDIX C: EVALUATION OF THE WALL HEAT TRANSFER COEFFICIENT FOR THE S2D MODEL

Under the comparison conditions between the 2R2D and S2D models in section 5 of the main text, it is recalled that the underlying formulation is given by eqs 12a–12e for the former and eqs 13a–13c for the latter.

If the occurrence of a chemical reaction ($Q \equiv (-\Delta H)r_c = 0$ in eqs 12a, 12c and eq 13a) is neglected, the fluid stream in the bed simply exchanges heat with the wall assumed to be at uniform temperature T_w . Under such conditions, the solution of eqs 13a and 13c for the S2D model can be expressed by a well-known series, which for uniform inlet radial profile ($T = T_0$ at $z = 0$) can be written in terms of the cross-section average temperature \bar{T} as

$$\frac{\bar{T}(z) - T_w}{T_0 - T_w} = 4Bi_w^2 \sum_{n=1}^{\infty} \frac{\exp[-4\lambda_{ef}\beta_n^2 z / (Gc_{pf}D_t^2)]}{\beta_n^2(Bi_w^2 + \beta_n^2)} \quad (\text{C1})$$

where $Bi_w = D_t h_w / (2\lambda_{ef})$ is the Biot number and β_n is the n th positive eigenvalue defined by the root of the expression

$$Bi_w J_0(\beta_n) = \beta_n J_1(\beta_n) \quad (\text{C2})$$

J_0 and J_1 are the zero- and first-order Bessel functions.

For axial positions far enough from the reactor inlet, only the term corresponding to the smallest eigenvalue β_1 in eq C1 is significant.

$$\frac{\bar{T}(z) - T_w}{T_0 - T_w} = 4Bi_w^2 \frac{\exp[-4\lambda_{ef}\beta_1^2 z / (Gc_{pf}D_t^2)]}{\beta_1^2(Bi_w^2 + \beta_1^2)} \quad (\text{C3})$$

The overall heat transfer coefficient h_T is defined from $q_w = h_T(T_w - \bar{T})$, and an overall heat conservation equation can be written on a differential length dz as $q_w dz = (1/4)(\pi D_t^2)Gc_{pf}d\bar{T}$. Then

$$h_T = \frac{D_t}{4} \frac{Gc_{pf}}{T_w - \bar{T}} \frac{d\bar{T}}{dz} \quad (\text{C4})$$

If C3 is used to evaluate \bar{T} and $d\bar{T}/dz$, the following expression results for h_T :

$$h_T = \lambda_{ef} \frac{\beta_1^2}{D_t} \quad (\text{C5})$$

The criterion employed to define the wall heat transfer coefficient h_w of the S2D model can now be stated as requiring that the S2D model presents the same heat transfer rate as the 2R2D model at large values of z . Equivalently, the same value of h_T (eq C4) is required for both models. To complete the formulation of this criterion, the 2R2D model's expression of \bar{T} is needed. The series solution of eqs 12a, 12c, and 12e has been given by Mariani et al.²¹ The expression—equivalent to C3—for the leading term of \bar{T} can be written as

$$\frac{\bar{T}(z) - T_w}{T_0 - T_w} = \Gamma_1 \exp[-4\lambda_{ef,c}\mu_1^2 z / (Gc_{pf}D_c^2)] \quad (C6)$$

where Γ_1 is a constant, irrelevant for the present purpose, $D_c = D_t - D_p$, and μ_1 is the leading eigenvalue, which satisfies

$$\begin{aligned} Bi_f J_0(\mu_1) \left(\mu_1^2 - \frac{D_t h_{wf}}{\lambda_{ef,c}} \frac{G_c(N-1)^2}{G_1(2N-1)} \right) \\ = \mu_1 J_1(\mu_1) \left(\mu_1^2 - \frac{D_c h_f + D_t h_{wf}}{\lambda_{ef,c}} \frac{G_c(N-1)^2}{G_1(2N-1)} \right) \end{aligned} \quad (C7)$$

where $Bi_f = D_c h_f / (2\lambda_{ef,c})$. Evaluating h_T from eq C4 by using eq C6 to evaluate \bar{T} and $d\bar{T}/dz$

$$h_T = \lambda_{ef,c} \frac{\mu_1^2}{D_t} \frac{GN^2}{G_c(N-1)^2} \quad (C8)$$

Finally, from eqs C5 and C8

$$\left(\frac{(N-1)\beta_1}{N\mu_1} \right)^2 = \frac{\lambda_{ef,c}}{\lambda_{ef}} \frac{G}{G_c} \quad (C9)$$

Equation C9 should be satisfied by finding the matching value of the S2D model's parameter h_w , which is denoted h_w^0 .

The second criterion mentioned in section 5 considers a uniform heat generation rate Q (per unit catalyst volume) in the heat conservation equations of the models, eqs 12a, 12c, and 13a, $Q \equiv (-\Delta H)r_c$. At constant T_w and high enough values of z , a stationary temperature profile develops, which allows transferring to the wall the whole amount of heat generated. Equation 12c (with $\partial T_c / \partial z = 0$) can be easily integrated and the amount of heat transferred at the boundary $\rho = \rho_c$ is then evaluated as

$$2\pi\rho_c h_c (\bar{T}_c - T_{c,1}) = \pi\rho_c^2 Q(1 - \varepsilon_c) \quad (C10)$$

where $h_c = 4\lambda_{ef,c}/\rho_c$. The thermal boundary condition in eq 12e becomes expressed as

$$2\pi\rho_c h_f (T_{c,1} - T_1) = \pi\rho_c^2 Q(1 - \varepsilon_c) \quad (C11)$$

The energy conservation equation in the wall channel (eq 12a), with $dT_1/dz = 0$, becomes

$$2\pi\rho_t h_{wf} (T_1 - T_w) = 2\pi\rho_c h_f (T_{c,1} - T_1) + \pi(\rho_t^2 - \rho_c^2) Q (1 - \varepsilon_1) \quad (C12)$$

The global heat transfer coefficient h_T is defined from

$$2\pi\rho_t h_T (\bar{T} - T_w) = \pi\rho_t^2 Q(1 - \varepsilon) \quad (C13)$$

From eqs C10–C13 and the definitions of G , ε and \bar{T} in section 5

$$\begin{aligned} h_T &= \frac{h_{wf}}{1 + \Psi}; \\ \Psi &= \left(\frac{\rho_c}{\rho_t} \right)^3 \left(\frac{G_c}{G} \right) \left(\frac{1 - \varepsilon_c}{1 - \varepsilon} \right) h_{wf} \left(\frac{1}{h_f} + \frac{1}{h_c} \right) \end{aligned} \quad (C14)$$

Following for the S2D model (formulated in eqs 13a–13c) similar considerations as for the 2R2D model and using definition C13, it follows that

$$h_T = \frac{h_w}{1 + h_w/h}; \quad h = 8\lambda_{ef}/D_t \quad (C15)$$

Equating h_T from eqs C14 and C15, h_w (denoted h_w^Q) can be evaluated as

$$h_w^Q = \frac{h_{wf}}{1 + \Psi - h_{wf}/h} \quad (C16)$$

From eq C13 we learn that by equating h_T the stationary value \bar{T} also becomes the same in both models.

AUTHOR INFORMATION

Corresponding Author

*E-mail: german.mazza@idepa.gov.ar.

Notes

The authors declare no competing financial interest.

ACKNOWLEDGMENTS

The authors wish to thank the Universidad Nacional de La Plata (PID 11/I177), Universidad Nacional del Comahue (PID 04/I158-2010-2012, PID 04/I191-2013-2016), ANPCyT-MINCYT (PIC11-1641), ANPCyT, PFDT-PRH 33 (FAIN-UNCO), and CONICET (PIP 0304) for providing financial support. G.D.M. and G.F.B. are research members of CONICET (Argentina).

NOMENCLATURE

- C = molar concentration of key reactant in the fluid, mol m⁻³
- $C_{c,1}$ = molar concentration of key reactant in the core channel at $\rho = \rho_c$, mol m⁻³
- C^s = molar concentration of key reactant on the catalyst surface, mol m⁻³
- c_{pf} = specific heat of the fluid, J kg⁻¹ K⁻¹
- D_e = radial effective diffusivity, m² s⁻¹
- D_t = tube diameter, m
- D_p = particle diameter, m
- f = catalyst activity factor
- G = specific mass flow rate (generic or average on the bed cross section), kg m⁻² s⁻¹
- L = spacing between parallel layers, m
- N = tube-to-particle diameter ratio ($=D_t/D_p$)
- Nu = Nusselt number (suffix is that of the heat transfer coefficient h) ($=hD_p/\lambda_f$)
- n_p = number of particle centers in the first layer per unit area of the cylindrical surface of radius ρ_c , m⁻²
- n_p^* = normalized density of particle centers ($=n_p D_p^2$)
- H = tube length, m
- h_f = heat exchange coefficient between the wall and core channels, W m⁻² K⁻¹
- h_{fs} = fluid–particle heat transfer coefficient, W m⁻² K⁻¹
- h_s = heat exchange coefficient between particle hemispheres, W m⁻² K⁻¹

h_{sL} = heat transfer coefficient between the solid core region and the facing particle hemisphere of the first layer, $W m^{-2} K^{-1}$
 h_w = wall-to-bed heat transfer coefficient in S2D model, $W m^{-2} K^{-1}$
 h_w^0 = value of h_w estimated without heat generation rate, $W m^{-2} K^{-1}$
 h_w^Q = value of h_w estimated with uniform heat generation rate, $W m^{-2} K^{-1}$
 h_{wf} = heat transfer coefficient across an unmixed fluid film on the wall, $W m^{-2} K^{-1}$
 h_{ws} = heat transfer coefficient between the wall and the facing particle hemisphere, $W m^{-2} K^{-1}$
 k = forward reaction rate coefficient in ammonia synthesis, $mol atm^{-1.5} m^{-3} s^{-1}$
 k' = reverse reaction rate coefficient in ammonia synthesis, $mol atm^{0.5} m^{-3} s^{-1}$
 Q = heat generation rate, $W m^{-3}$
 q = heat flux, $W m^{-2}$
 Re_p = Reynolds number ($=GD_p/\mu_f$)
 r_e = effective reaction rate (per unit volume of catalyst)
 T = fluid phase temperature, K
 $T_{c,1}$ = temperature in the core channel at $\rho = \rho_c$, K
 $T_{c,L}^s$ = particle surface temperature in solid core region at $\rho = \rho_L$, K
 T^s = particle surface temperature, K
 $u(y^*)$ = local superficial axial velocity as a function of y^* , $m s^{-1}$
 V_p = particle volume, m^3
 x = N_2 conversion ($=1 - C/C_i$)
 y^* = dimensionless distance from the wall ($=y/D_p$)
 y_L^* = value of y^* where the solid core region begins in present 2R2D model (eq 4a)
 y_w^* = value of y^* where the core region begins in 2R2D models
 z = axial coordinate, m
 z^* = dimensionless axial coordinate ($=z/H$)

Greek Symbols

α_f = mass exchange coefficient between the wall and core channels, $m s^{-1}$
 ΔH = heat of reaction, $J mol^{-1}$
 δ_f = fluid density, $kg m^{-3}$
 ε = void fraction (generic or average on the bed cross section)
 λ_e = effective radial thermal conductivity of the bed, $W m^{-1} K^{-1}$
 λ_{e0} = static contribution (without fluid flow) to λ_e , $W m^{-1} K^{-1}$
 λ_{eD} = fluid-dispersion contribution to λ_e , $W m^{-1} K^{-1}$
 λ_{ef} = contribution of fluid to λ_e , $W m^{-1} K^{-1}$
 λ_{es} = contribution of particles to λ_e , $W m^{-1} K^{-1}$
 λ_f = fluid thermal conductivity, $W m^{-1} K^{-1}$
 μ_f = fluid viscosity, $kg m^{-1} s^{-1}$
 ρ = radial coordinate, m
 ρ_c = radial coordinate at $y^* = 1/2$, m
 ω = fraction of particle volume intersected in $0 < y^* < 1/2$

Subscripts and Superscripts

1 = average quantity evaluated in $1 < y^* < 1/2$
 2 = average quantity evaluated in $1/2 < y^* < y_L^*$
 2R = evaluated by 2R2D model
 ax = quantity evaluated at the tube axis
 c = relative to the core channel or core solid region
 I = quantity evaluated at reactor inlet
 L = quantity evaluated at y_L^*
 S0 = evaluated by S2D model using coefficient h_w^0
 SQ = evaluated by S2D model using coefficient h_w^Q
 t = quantity evaluated at the tube wall

– = mixing-cup average quantity
 w = quantity evaluated at the tube wall

REFERENCES

- (1) Coberly, C. A.; Marshall, W. R. Temperature gradients in gas streams flowing through fixed granular beds. *Chem. Eng. Prog.* **1951**, *47*, 141.
- (2) Brötz, W. Untersuchungen über wärmeleitung, stofftransport und druckabfall in durchströmten schüttungen. *Chem. Eng. Technol.* **1951**, *23*, 408.
- (3) Dixon, A. G. Fixed bed catalytic reactor modeling—The radial heat transfer problem. *Can. J. Chem. Eng.* **2012**, *90*, 507.
- (4) Mueller, G. E. Angular Void Fraction Distributions in Randomly Packed Fixed Beds of Uniformly Sized Spheres in Cylindrical Containers. *Powder Technol.* **1993**, *77*, 313.
- (5) Salvat, W. I.; Mariani, N. J.; Barreto, G. F.; Martinez, O. M. An algorithm to simulate packing structure in cylindrical containers. *Catal. Today* **2005**, *107–108*, 513.
- (6) Giese, M.; Rottschäfer, K.; Vortmeyer, D. Measured and modeled superficial flow profiles in packed beds with liquid flow. *AIChE J.* **1998**, *44*, 484.
- (7) Tsotsas, E.; Schlünder, E.-U. Heat transfer in packed beds with fluid flow: remarks on the meaning and the calculation of a heat transfer coefficient at the wall. *Chem. Eng. Sci.* **1990**, *45*, 819.
- (8) Li, C. H.; Finlayson, B. A. Heat transfer in packed beds—A reevaluation. *Chem. Eng. Sci.* **1977**, *32*, 1055.
- (9) Zambon, M. T. Ph.D. Thesis, Faculty of Engineering, National University of La Plata, Argentina, 2010.
- (10) Ahmed, M.; Fahien, R. W. Tubular reactor design—I: two-dimensional model. *Chem. Eng. Sci.* **1980**, *35*, 889.
- (11) Botterill, J. S. M.; Denloye, A. O. O. A theoretical model of heat transfer to a packed or quiescent fluidized bed. *Chem. Eng. Sci.* **1978**, *33*, 509.
- (12) Gunn, D. J.; Ahmad, M. M.; Sabri, M. N. Radial heat transfer to fixed beds of particles. *Chem. Eng. Sci.* **1987**, *42*, 2163.
- (13) Borkink, J. G. H.; Westerterp, K. R. Significance of the radial porosity profile for the description of heat transport in wall-cooled packed beds. *Chem. Eng. Sci.* **1994**, *49*, 863.
- (14) Legawiec, B.; Ziółkowski, D. Mathematical simulation of heat transfer within tubular flow apparatus with packed bed by a model considering system inhomogeneity. *Chem. Eng. Sci.* **1995**, *50*, 673.
- (15) Winterberg, M.; Tsotsas, E.; Kriskchke, A.; Vortmeyer, D. A simple and coherent set of coefficients for modelling of heat and mass transport with and without chemical reaction in tubes filled with spheres. *Chem. Eng. Sci.* **2000**, *55*, 967.
- (16) Smirnov, E. I.; Muzykantov, A. V.; Kuzmin, V. A.; Kronberg, A. E.; Zolotarskii, I. A. Radial heat transfer in packed beds of spheres, cylinders and Rashig rings. Verification of model with a linear variation of λ_{ef} in the vicinity of the wall. *Chem. Eng. J.* **2003**, *91*, 243.
- (17) Magnico, P. Pore-scale simulations of unsteady flow and heat transfer in tubular fixed beds. *AIChE J.* **2009**, *55*, 849.
- (18) Ranz, W. E. Friction and transfer coefficients for single particles and packed beds. *Chem. Eng. Prog.* **1952**, *48*, 247.
- (19) Baron, T. Generalized graphical method for the design of fixed bed catalytic reactors. *Chem. Eng. Prog.* **1952**, *48*, 118.
- (20) Winterberg, M.; Tsotsas, E. Correlations for effective heat transport coefficients in beds packed with cylindrical particles. *Chem. Eng. Sci.* **2000**, *55*, 5937.
- (21) Mariani, N. J.; Mazza, G. D.; Martinez, O. M.; Cuckierman, A. L.; Barreto, G. F. On the influence of liquid distribution on heat transfer parameters in trickle bed systems. *Can. J. Chem. Eng.* **2003**, *81*, 814.
- (22) Martin, H. Low Peclet number particle-to-fluid heat and mass transfer in packed beds. *Chem. Eng. Sci.* **1978**, *33*, 913.
- (23) Yagi, S.; Kunii, D. Studies on heat transfer near wall surface in packed beds. *AIChE J.* **1960**, *6*, 97.
- (24) Legawiec, B.; Ziółkowski, D. Structure, voidage and effective thermal conductivity of solids within near-wall region of beds packed with spherical pellets in tubes. *Chem. Eng. Sci.* **1994**, *49*, 2513.

(25) Mariani, N. J.; Salvat, W. I.; Martinez, O. M.; Barreto, G. F. Packed bed structure. Evaluation of radial particle distribution. *Can. J. Chem. Eng.* **2002**, *80*, 186.

(26) Bey, O.; Eigenberger, G. Fluid flow through catalyst filled tubes. *Chem. Eng. Sci.* **1997**, *52*, 1365.

(27) Gunn, D. J. Transfer of heat or mass to particles. *Int. J. Heat Mass Transfer* **1978**, *21*, 467.

(28) Bauer, R.; Schlünder, E.-U. Effective radial thermal conductivity of packings in gas flow. Part II Thermal conductivity of the packing fraction without gas flow. *Int. Chem. Eng.* **1978**, *18*, 189.

(29) Nijemeisland, M.; Dixon, A. G. Comparison of CFD simulations to experiment for convective heat transfer in a gas-solid fixed bed. *Chem. Eng. J.* **2001**, *82*, 231.

(30) Romkers, S.; Dautzenberg, F.; van den Bleek, C.; Calis, H. CFD modeling and experimental validation of particle-to-fluid mass and heat transfer in a packed bed at very low channel to particle diameter ratio. *Chem. Eng. J.* **2003**, *96*, 3.

(31) Bai, H.; Theuerkauf, J.; Gillis, P. A coupled DEM and CFD simulation of flow field and pressure drop in fixed bed reactor with randomly packed catalyst particles. *Ind. Eng. Chem. Res.* **2009**, *48*, 4060.

(32) Villadsen, J.; Michelsen, M. L. *Solution of Differential Equation Models by Polynomial Approximation*; Prentice Hall: Upper Saddle River, NJ, 1978.

(33) Barreto, G. F.; Mazza, G. D. On the use of incremental quotients in Michelsen's method for stiff ordinary differential equations. *Comput. Chem. Eng.* **1989**, *13*, 967.

(34) Temkin, M. I.; Pyzhev, V. Kinetics of the synthesis of ammonia on promoted iron catalysts. *J. Phys. Chem. (Moscow, Russ. Fed.)* **1939**, *13*, 851.

(35) Mariani, N. J.; Mazza, G. D.; Martinez, O. M.; Barreto, G. F. The distribution of particles in cylindrical packed beds. *Trends Heat Mass Transfer* **1998**, *4*, 95.

(36) Bey, O.; Eigenberger, G. Gas flow and heat transfer through catalyst filled tubes. *Int. J. Therm. Sci.* **2001**, *40*, 152.